Hindawi
Geofluids
Volume 2022, Article ID 1101015, 21 pages
https://doi.org/10.1155/2022/1101015

Research Article

Hydrogeochemical Characteristics and Geothermometry of Hot Springs in the Tensile Tectonic Region Leizhou Peninsula and Hainan Island in South China

Hongyu Hu,[1] **Guoping Lu**,[2] **Qiuying Lu**,[3] **Yan Li**,[2] **Linjun Xie**,[1] **Xuanhao Lin**,[2] **Ming Wu**,[2] **Cehui Mo**,[2] **and Bei Zhang**[1]

[1]*School of Environment, Jinan University, Guangzhou, Guangdong 510632, China*
[2]*College of Life Science and Technology, Jinan University, 601 Huangpu Ave West, Guangzhou, Guangdong 510632, China*
[3]*School of Computer and Information Engineering, Hubei University, Wuhan, Hubei 430062, China*

Correspondence should be addressed to Guoping Lu; guopinglu@yahoo.com and Yan Li; liyan9636@126.com

Received 28 September 2021; Revised 22 January 2022; Accepted 10 February 2022; Published 16 March 2022

Academic Editor: Jean-Luc Michelot

Hydrochemistry and isotopes are studied for characterizations of geothermal waters, groundwaters, and surface waters in Leizhou Peninsula (LZ) and the northern part of Hainan Island (HN) across the tensile-tectonic Qiongzhou Strait, southern China. Water chemistry results showed that most geothermal waters are of alkaline and HCO_3-Na types, while shallow groundwater samples were significantly different with HCO_3-Ca, HCO_3-Mg, and HNO_3-Ca types. Stable isotope data indicated that the source of LZ geothermal waters is of atmospheric precipitation, while HN geothermal water has a slight "oxygen drift". Cation geothermometers and silica geothermometers could appropriately predict reservoir temperatures. Based on multicomponent mineral equilibria and quart geothermometer without steam loss, reservoir temperatures were estimated to be in the range of 65.0°C to 165.0°C at an average circulation depth of 2023 m, substantiated with data from a thousand-meter-depth borehole. The saturation indexes (SI) simulated by PHREEQC and Na-K-Mg triangle diagram revealed that the chemical components in the geothermal waters are possibly derived from water-rock interactions at high temperatures. Four simulation paths were established to calculate the mass flux of minerals by PHREEQC program. The hydrothermal circulation process of the volcanic rocks on both sides of the Qiongzhou Strait was similar, but the water-mineral reactions of Leizhou Peninsula were more intense. During the high-temperature hydrothermal deep circulation in the central part of Hainan Island, the molar transfer was low and the degree of mineral reaction is weak. Finally, the geothermal genetic mechanism for the study area of the extensional geostructure was proposed. The findings mark the characteristics for the tensile-tectonic region in slight "oxygen shift", low values of $^{87}Sr/^{86}Sr$ for possible deep source from the mantle, and higher reservoir temperatures at shallower circulation depths.

1. Introduction

Our study area is located at the Leizhou Peninsula and northern Hainan Island, crossings Qiongzhou Strait in southern China. The Qiongzhou Strait is tectonically of tensile geostructure nature, connecting the Beibu Bay (to the west) and to the South China Sea. It has a long history of exploitation and utilization of geothermal water and is a famous sanatorium [1]. Geothermal system is formed under complex natural environmental conditions. Geological structures and hydrogeological conditions can control the formation of geothermal systems. Therefore, understanding the formation mechanism, storage environment, and heat-mass transport of geothermal resources is the necessity to aid the development and protection of these geothermal resources [2, 3].

With increasing demand for resources in recent years, geothermal resources have attracted more and more attention, over the use of traditional nonrenewable energy such as oil and coal leading to a series of environmental problems [4]. As a renewable energy source, geothermal resource has

the unique advantages of cleanness, utilization, environmental protection, stability, and natural medical value compared to other energy sources [5]. China is a country with abundant geothermal resources for huge potential development and utilization. In 2020, the utilization of geothermal energy accounted for 1.5% of Chinese primary energy. Therefore, the development of geothermal energy has important significance for alleviating energy pressure, improving ecological environment, and promoting energy revolution [6, 7]. Geothermal waters can be used not only for heating, bathing, and health care but also for power generation. Therefore, the development of geothermal water is of great significance to the promotion of local economies. In the process of long-term geothermal energy utilization, the development of geothermal energy has been hindered by problems such as low utilization rates, blind development, and environmental aggravation.

The Leizhou Peninsula (LZ) and northern Hainan Island (HN) are famous for their tourism industry. Countless tourists from all over the world come here during the peak season. The development of geothermal resources in the study area will extremely promote local economic development [8, 9]. Heating is one of the most important development and utilization methods of geothermal resources, which accounts for 32.7% of the total utilization of geothermal resources in China [6]. But the typical tropical and subtropical climates in the study area make it less attracting to be used for heating and drying, which somehow restricts the development and utilization of geothermal water. Hot spring tourism is becoming an important industry in HN, which makes great contributions to the local economy. However, the problems arise, such as environmental pollution and unscientific exploitation of geothermal resources, and have increasingly threatened development of the local tourism [10].

It has long been suspected that the tensile geostructures in the regions have controlled and underlined the geothermal occurrences, and however, little work has been done. Some work has been conducted in detailed analysis on the geological and hydrological conditions and the storage, source, and cover characteristics of the hydrothermal systems of Leizhou Peninsula (LZ) and northern Hainan Island fields (HN) [11–13]. Zhou et al. [14] established LZ groundwater model to control seawater intrusion and provide scientific guidance for rational use of groundwaters. Zhang et al. [15] studied the water chemistry and isotopic characteristics in LZ and revealed the main hydrogeochemical processes that control water quality. Yao et al. [16] simulated water-rock interaction processes by PHREEQC geochemical models and revealed the evolution mechanism of groundwater chemical environment in the study area. Zhang [17] conducted a survey of most hot springs in Hainan Province and systematically analyzed their characteristics and origins. However, geothermal waters located on both sides of the strait, where hot springs occur in areas with volcanic eruptions in geological history, have seldom been studied. Questions regarding overall characteristics and their relevance to the regional geological structures in the geothermal system are still unknown.

The objectives of this study are to reveal the processes controlling the hydrogeochemical evolution of geothermal waters and to improve research on the genetic mechanism of the hydrothermal system in the extensional geostructure area. In this paper, we conducted hydrochemical, isotopic, and geological characterizations of the geothermal waters, to understand the processes of the deep regional groundwater flow system. Thermal reservoir temperature estimations were calculated, based on three temperature estimation methods, and their applicability could provide references for their applications to other similar regional-scale deep geothermal flow system. We have significantly improved the research on the evolution mechanism of the study area, through quantification by hydrogeochemical calculations together with the evaluation on the water-rock reaction mechanism in the process of geothermal water flow, which can provide solutions for the sustainable exploitation, management, and utilization of geothermal water.

2. Study Area

The study area covers the Leizhou Peninsula and the northern part of Hainan Island (109°23′31″-110°41′17″, 19°6′48″-22°16′13″) (Figures 1(a) and 1(b)). LZ has a tropical monsoon climate, with an average annual temperature of about 23.0°C and a monthly average temperature of 14.5°C-29.0°C. The elevation of the peninsula ranges from 240 to 275m in the central parts of the peninsula to a few meters along the coast [18]. LZ is exposed dominantly as volcanic rock platforms and eroded accumulation plains and coastal marine plains as well. The volcanic rock platforms in the north and south have higher terrain, and the platforms decrease in height from the crater to the surroundings. Accumulation plains are mainly distributed in the area from the north of LZ to the south of Suixi County (Figure 1(c)).

The Leizhou Peninsula has experienced four tectonic periods: Caledonian, Hercynian-Indosinian, Yanshanian, and Himalayan. The geological structure is relatively complex. Bedrock units in LZ are mainly of Cambrian and Cretaceous strata, which are covered by unconsolidated alluvial and lacustrine sediments. Cretaceous bedrocks are composed mainly of gray conglomerates, sandstones, and siltstones, while Cambrian purple sandstones are interbedded with mudstone and marls. The unconsolidated sedimentary rocks include coarse sands with gravels and scattered lenses of clay and an upper layer of clay of the Zhanjiang Group of Quaternary system (Q). And Cenozoic Basalts are formed by volcanic eruption in the Himalayas (β) (Figure 1(d)) [19].

Professor Li Dewei was in charge of a hot dry rock drilling project successfully drilled down to 4387 m in depth, as in the borehole bottom temperature as high as 185°C in the Huadong basin in northern Hainan Island in March 2018 (Figure 1(d)). It is worth noting that the geographical features in HN are very similar to those of LZ, with track of basalts formed by volcanic eruptions. The strata outcropping in HN include Silurian sandstone and slate, Cenozoic basalt, Quaternary clay and sand, Cretaceous quartz clastic rock, and Mesozoic granite. In study area, four groups of active

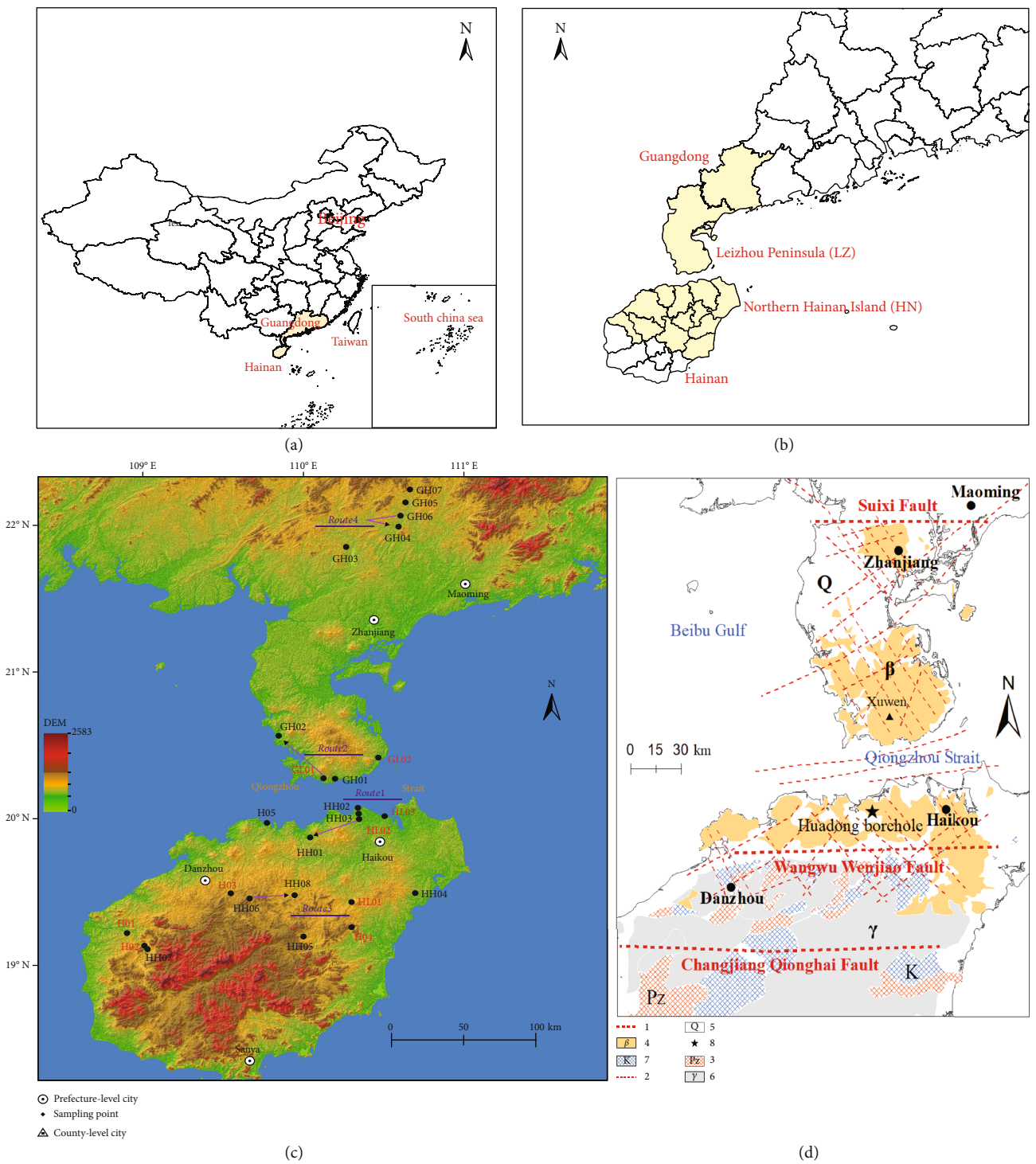

Figure 1: Location and regional geological sketch of the study area. 1-Fault; 2-probable fault; 3 Paleozoic; 4-Cenozoic basalt; 5-Quaternary clay and sand; 6-Mesozoic granite; 7-Cretaceous quartz clastic rock; and 8-4387 m Huadong hot dry rock borehlole, and the drilling temperature is 185°C.

faults can be identified, which include nearly EW-trending, NE-trending, NEE-trending, and NW-trending faults. EW-trending faults play an important role in the crustal movement. Furthermore, the EW-trending Wangwu-Wenjiao fault controlled the Cenozoic deposition and volcanic activities of the study area (Figure 1(d)) [20].

3. Materials and Methods

A total of 25 samples were collected from LN and HN in July 2019, including 15 thermal spring samples, 5 groundwater samples, 1 rainwater sample, 1 seawater sample, and 3 river water samples. Water samples were stored in polyethylene

Table 1: Concentrations of major chemical constituents of the water samples from study area. (Concentrations in mg/L).

Sample	Sample type	pH	T/°C	TDS	K	Na	Ca	Mg	Cl	HCO_3	NO_3	F	Br	SiO_2	d^2H	$\delta^{18}O$	$^{87}Sr/^{86}Sr$	Hydrochemical type
Thermal waters																		
GH01	LZ	8.36	43.6	409	3.51	192.3	3.59	0.36	12.00	480.22	5.53	0.47	0.099	25.60	-50.7	-7.52	0.7094	HCO_3-Na
GH02	LZ	8.22	39.5	301	4.76	132	12.85	1.45	21.3	323.78	5.35	0.24	0.099	24.56	-51.7	-7.34	0.7098	HCO_3-Na
GH03	LZ	7.18	56.8	221	4.02	95.25	18.56	0.14	7.86	87.94	12.40	17.50	0.023	104.64	-40.3	-6.16	0.7131	HCO_3-Na
GH04	LZ	9.06	37.0	316	1.89	95.35	1.74	0.15	10.25	76.34	10.48	14.74	0.038	70.16	-42.1	-6.61	0.7155	HCO_3-Na
GH05	LZ	6.67	49.1	273	25.14	250.18	98.66	11.3	11.51	233.55	57.19	6.33	0.029	98.42	-44.4	-6.74	0.7368	HCO_3-Na
GH06	LZ	9.14	33.4	230	3.27	102.87	1.71	0.08	11.82	93.56	10.42	17.17	0.029	96.34	-39.3	-6.04	0.7178	SO_4-Na
GH07	LZ	7.47	50	361	6.10	173.58	15.62	0.23	9.49	153.47	21.83	10.22	0.024	108.55	-42.2	-6.37	0.7413	HCO_3-Na
HH01	HN	8.1	35.1	746	5.14	778.12	4.78	1.45	310.34	1122.3	257.78	6.32	1.250	28.21	-49.4	-6.53	0.7100	HCO_3-Na
HH02	HN	7.99	43.8	1430	6.00	681.25	4.18	2.18	383.38	1106.00	6.4	7.36	1.959	26.70	-43.6	-6.48	0.7099	HCO_3-Na
HH03	HN	8.47	38.7	1306	4.91	653.75	2.99	1.09	290.61	1058.7	6.33	8.29	1.128	25.54	-42.7	-6.37	0.7102	HCO_3-Na
HH04	HN	7.59	70.1	3096	63.25	960	293.42	0.013	1957.3	71.85	0.05	5.30	9.415	106.95	-46.9	-6.18	0.7131	Cl-Na
HH05	HN	8.92	47.3	266	3.06	125.5	4.18	0.013	19.07	83.67	0.05	22.00	0.042	96.08	-52.8	-7.38	0.7094	SO_4-Na
HH06	HN	8.18	83.5	281	5.75	114.75	10.76	1.09	21.46	125.51	0.05	20.40	0.055	131.71	-54.8	-6.98	0.7122	HCO_3-Na
HH07	HN	9.07	40.1	442	2.55	110.5	2.39	0.36	8.65	77.31	0.99	23.10	0.022	73.83	-65.5	-8.92	0.7126	HCO_3-Na
HH08	HN	8.19	55.4	131	3.04	112	4.78	0.72	19.70	130.97	0.05	21.25	0.053	74.61	-55.3	-7.41	0.7114	HCO_3-Na
Cold waters																		
GL01	groundwater	6.79	27.6	470	2.88	18.43	34.66	19.57	33.07	76.40	123.39	0.02	0.114	66.26	-59.0	-7.72	0.7035	NO_3-Ca
GL02	groundwater	6.81	35.1	102	0.97	17.83	5.98	4.71	30.75	17.28	3.7	0.02	0.119	4.85	-43.5	-5.88	0.7102	Na-Cl
HL01	groundwater	6.89	26.1	221	1.00	9.16	17.93	10.88	8.09	102.77	15.17	0.02	0.040	50.54	-44.9	-6.7	0.7040	HCO_3-Mg
HL02	groundwater	6.93	26.3	668	3.62	3.98	4.18	0.36	2.99	32.74	—	0.02	25.500	—	-23.5	-3.42	—	HCO_3-Na
HL03	groundwater	7.85	26.5	3490	3.52	9.54	9.56	3.26	12.97	36.38	—	0.42	43.700	17.35	-36.5	-5.1	—	HCO_3-Na
H01	surface water	7.59	28.7	421	2.72	6.87	10.76	2.18	5.40	46.38	1.85	0.44	0.034	—	-39.2	-5.45	0.7131	HCO_3-Ca
H02	surface water	7.25	27.6	380	0.92	4.69	9.56	1.81	3.18	40.02	1.43	0.26	0.030	—	-38.8	-5.51	0.7028	HCO_3-Ca
H03	surface water	6.85	27.5	329	2.60	7.15	8.37	2.00	7.22	38.20	0.05	0.32	0.041	—	-34.4	-4.97	0.7101	HCO_3-Ca
H04	rainwater	8.15	27.8	101	7.96	632.5	29.88	14.5	466.6	656.66	3.17	1.98	2.277	—	-47.4	-6.67	—	Cl-Na
H05	seawater	7.15	27.1	1001	14.11	488.75	19.72	57.28	857.80	10.91	1.18	0.02	3.965	—	—	—	0.7092	Cl-Na

bottles, including one (500 mL) bottle and two smaller (50 mL) bottles that had been rinsed with water sample three times before sampling. All the water chemical samples were filtered through 0.45 μm membranes on site. Unstable hydrochemical parameters including temperature, pH, oxidation-reduction potential (Eh), dissolved oxygen (DO), and electrical conductivity (EC) were measured with a WTW Multi 3400i multiparameter portable field meter. Total alkalinity in samples was measured by the volumetric method (NaOH titration) using phenolphthalein as an indicator. Ultrapure dilute nitric acid was used to acidify a portion of the samples to pH<2 for the analyses of major cations and trace elements.

Determinations of the anions, cations, and trace elements were carried out using Flame spectrophotometer (FP6410), Atomic absorption spectrometer (Thermo ICE 3500), and Ion chromatograph (ICAP Q) in Karst Geological Resources Environmental Supervision and Inspection Center of the Ministry of Land and Resources, China (KGRE). The repeated detection error of cations and anions does not exceed ±1%, with the detected accuracy about 0.001 mg/L.

The δ^2 H and δ^{18}O stable isotope compositions in water samples were measured by using the IMAT253 stable isotope mass spectrometer (MAT253) in KGRE. The results were reported relative to SMOW standard, and the errors were about ±0.5‰ (δ^2 H) and ±0.05‰ (δ^{18}O) measured in the laboratory, respectively. The $^{87}Sr/^{86}Sr$ ratio was analyzed using the isotope mass spectrometer (MAT-261) at the State Key Laboratory of Geological Process and Mineral Resources in Wuhan, China, University of Geosciences.

4. Results

4.1. Water Chemical Composition. The measured temperatures of thermal and cold groundwaters varied from 33.4°C to 83.5°C and from 26.1°C to 27.6°C, respectively (Table 1). The temperature of geothermal water ranges from 33.4°C to 56.8°C in LZ and from 35.1°C to 83.5°C in HN. It is not difficult to conclude that the geothermal fields in the study area are typical mid-low temperature geothermal fields. The pH values of all the geothermal waters varied from neutral to alkaline, while the cold groundwaters pH are nearly neutral with the pH ranging from 6.79 to 7.85. For the geothermal water samples, LZ and HN have pH 8.01 and 8.31 on average, respectively. The TDS of the geothermal waters ranges from 131 mg/L to 3096 mg/L, while cold groundwater showed different concentrations with TDS ranging from 221 to 3490 mg/L. The TDS are significantly higher in HN (mean 962.25 mg/L) than in LZ (mean 301.57 mg/L).

There are large differences in the hydrochemical compositions of water samples collected from the HN and LZ. In these two regions, Cl and Na were the main anion and cation in solution, respectively. Na average content exceeds 900 mg/L in the thermal groundwaters (95.25-250.18 mg/L and 110.50-960.00 mg/L in LZ and HN, respectively), but less than 20 mg/L in cold groundwaters. HCO_3 contents of geothermal water are 76.34-480.22 mg/L and 71.85-1122.30 mg/L in LZ and HN, respectively, but are in the range of 17.28-102.77 mg/L overall in cold groundwaters. Ca contents are 1.71-98.66 mg/L and 2.39-293.42 mg/L in the LZ thermal springs and HN thermal springs, respectively, but only 4.18-34.66 mg/L overall in the cold groundwaters. Cl contents are 7.86-1957.30 mg/L in the thermal groundwaters (7.86-30.07 mg/L and 8.65-1957.30 mg/L in LZ and HN, respectively) and 2.99-33.07 mg/L in the cold groundwaters. Similarly, dissolved SiO_2 contents are 24.56-131.71 mg/L in the thermal groundwaters. For minor ions, the F content in the geothermal waters is significantly higher than in the groundwaters and the surface waters. The F content of Cl-Na type geothermal water is significantly higher than that of HCO_3-Na type, with an average of 19.59 mg/L and 10.10 mg/L, respectively. On the contrary, the Br content of HCO_3-Na type geothermal water is higher than that of Cl-Na type, especially in Hainan Island.

4.2. Isotope Compositions. The thermal and cold groundwaters showed great differences in δ^2 H and δ^{18}O values. The stable isotope contents for all the sampled hot waters range from -8.92‰ to -5.88‰ for δ^{18}O and from -65.5‰ to -39.3‰ for δ^2H, with an average of -6.81‰ and -47.8‰, respectively. The $\boldsymbol{d}^{18}$O and $\boldsymbol{d}^{2}$H values of cold groundwaters (-5.7‰ and -40.5‰ on average) are significantly lower than those of hot waters. For the Sr isotopes, the $^{87}Sr/^{86}Sr$ ratios of the geothermal waters in LZ are between 0.70943 and 0.74131, with an average value of 0.72053. The $^{87}Sr/^{86}Sr$ ratio average of the geothermal waters in HN is slightly smaller than in LZ, but the distribution is more concentrated, between 0.70279 and 0.71312. It is not difficult to find that the $^{87}Sr/^{86}Sr$ ratio of hot waters in the study area from the coast to the inland area shows a slight increase.

5. Discussions

5.1. Hydrochemical Characteristics of the Geothermal Waters

5.1.1. Hydrogeochemical Characteristics. Most geothermal water samples collected from LZ have the hydrochemistry type of HCO_3-Na, same as those from HN. In these two regions, HCO_3 and Na were the main anion and cation in solution, respectively. For other geothermal water samples, HH04 belongs to Cl-Na type while GH06 and HH05 are of SO_4-Na type. However, cold groundwaters and surface water have slightly different types of water chemistry. The hydrochemical type of all surface water samples is HCO_3-Ca, while groundwater samples include HCO_3-Ca, HCO_3-Mg, Cl-Na, and HNO_3-Ca types (Figure 2).

In the thermal water samples, major ions have higher concentrations than those in the cold groundwater and surface water. This is likely related to the long-term deep circulation of geothermal waters along fault systems, which allow more complete fluid-rock interactions (Figure 3). Some major ions are well correlated against TDS for different water samples. TDS is well correlated with Cl and Na in water sample, showing that water-rock interaction at high temperature may be the main source of the chemical components of thermal groundwaters [21]. Based on the

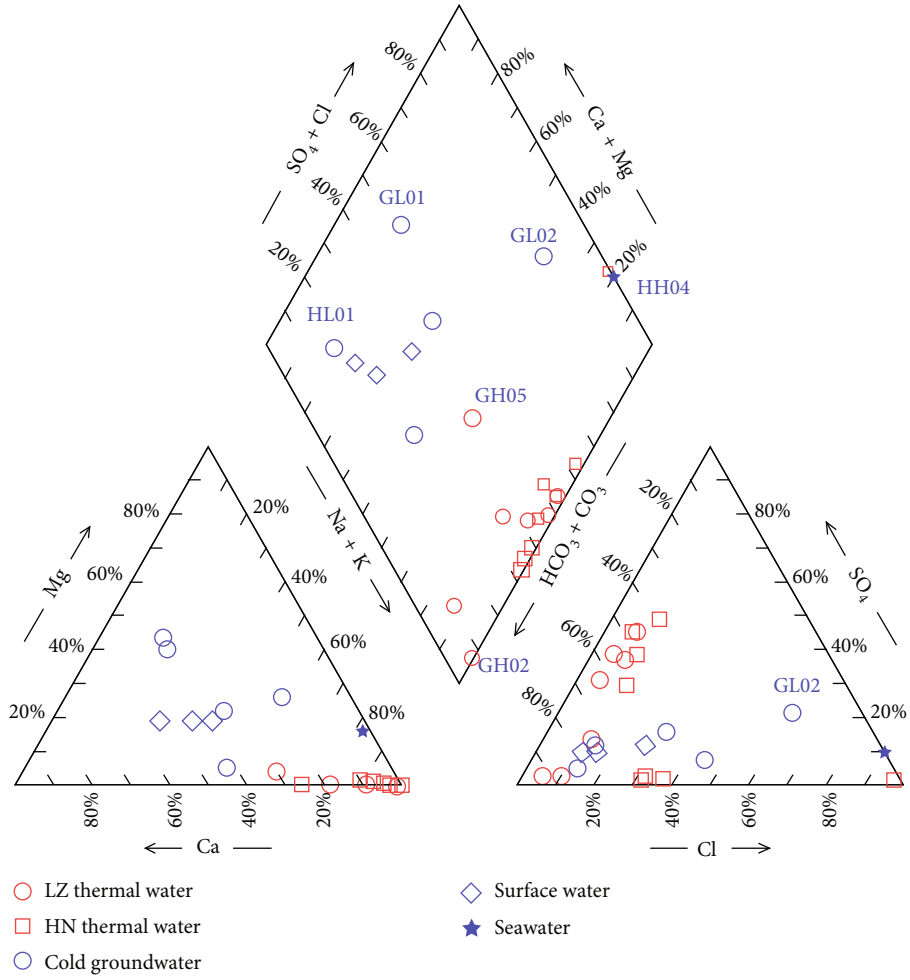

Figure 2: Piper diagram showing the water samples in the study area.

correlation between TDS and Cl (Figure 4), it can be concluded that thermal water and cold water are mixed in upper zones, which leads to the formation of intermediate thermal waters [22]. Cl is a typical natural tracer, often used to reflect the entire groundwater cycle process, including atmospheric source's infiltration, the leaching of evaporative salt rocks in aquifers, and geothermal water mixing with water from other sources [23].

The Cl content of geothermal waters in the study area is significantly higher than that of groundwaters and has a significant correlation with TDS. Based on the geological situation, the source of Cl ions may be atmospheric precipitation and the leaching of chloride-containing minerals in the groundwaters and atmospheric precipitation. The relationship between TDS and Ca is closely related to its formation conditions, and the Ca content of the geothermal water is higher than that of the groundwater. Enrichment of the high content Ca in hot waters can be attributed to cation exchange processes between geothermal fluids and silicate minerals under higher temperature and pressure conditions [24]. Silicon generally exists in the form of oxygen-containing compounds in nature, and SiO_2 content is mainly measured by the concentration of metasilicic acid in groundwater. The source of metasilicic acid is mainly the hydrolysis of aluminosilicate, and its solubility is affected by temperature and pressure. Within a certain range, the higher the temperature, the higher the content of SiO_2 in groundwater, so SiO_2 has higher content in the thermal groundwaters and higher relationship with TDS for all the groundwater samples (Figure 4).

5.1.2. Trace Elements. Most trace elements have higher concentrations in the geothermal waters than in the cold waters and surface waters. Temperature and pressure play a dominant role in controlling the release of trace elements. In the study area, it is worth noting that Li, B, Br, and F are abundant in the thermal water samples, and the presence of these elements has been identified in other geothermal fields, including Shenzao, Xinzhou, and Longmuwan geothermal fields [5, 25]. The Cl-Na type of thermal waters (as in the HH04 spring in HN) has a high B content and low Mg concentration. Some scholars have shown that the source of the type may come from the deep circulation of these waters through the crust and a water-rock interaction at high temperatures [26, 27]. The thermal water and regional flows are enriched with Li, which is the result of high geothermal mobility. In Jungapeo (Mexico), concentrations of B in geothermal waters ranged from 3.0-4.1 mg/L and Li from 0.23-

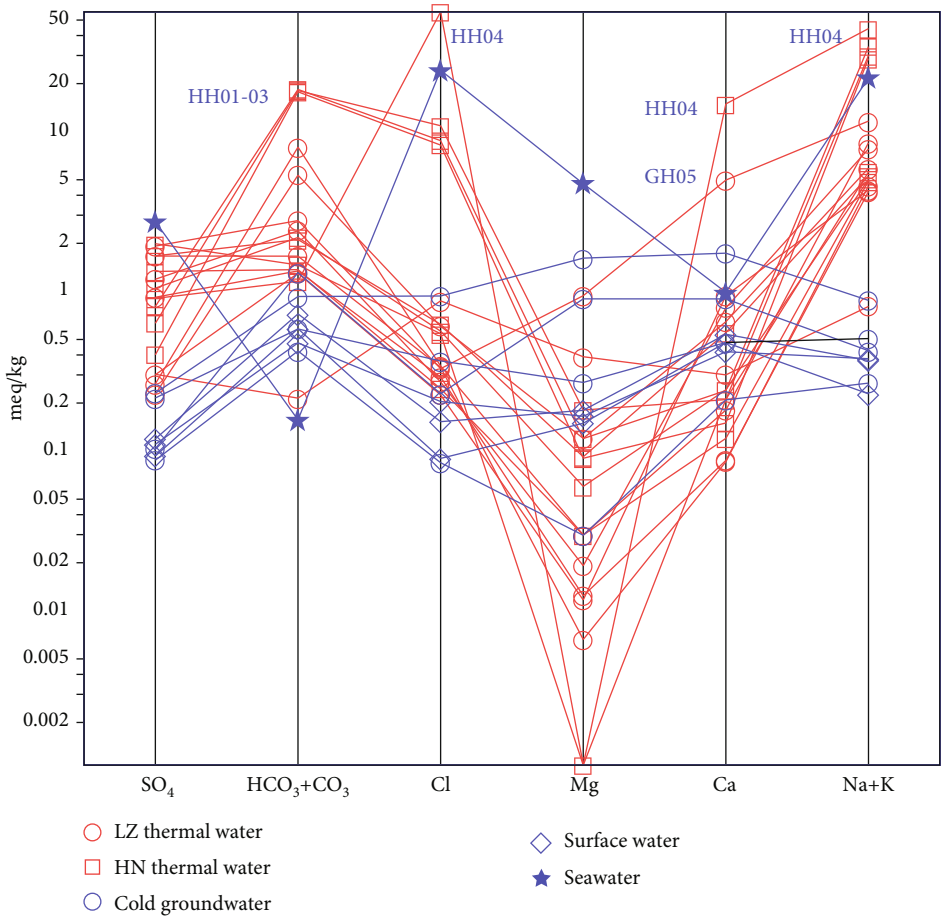

Figure 3: Schoeller diagram showing main ions constituents of the water samples.

2.03 mg/L. Siebe et al. revealed that the source of these waters is the mixing of meteoric water with CO_2–enriched thermal waters, the latter resulting from the regional flow and a remnant of heat from a basaltic magma body [28].

F as an essential trace element for the human body, and proper intake can effectively prevent diseases such as dental caries and osteoporosis, while excessive intake can lead to diseases such as fluorosis [29]. As shown in Figure 5, geothermal water F levels are positively correlated with pH and temperature. F and OH have the same radius and charges, and geothermal water OH often exchanges F in minerals, resulting in the increase of F concentration with the increase of pH. The enrichment processes of fluorine in groundwaters mainly include dissolution and precipitation, adsorption and desorption, and cation exchange, which will be strongly enhanced in the weak alkaline and high temperature environment in the study area. The fluorine content in the water samples is closely related to the hydrochemical type of the geothermal water, and the Cl-Na type geothermal water in the study area has a higher fluoride ion concentration. The Cl-Na type geothermal water has been in the slow groundwater flow zone for a long time, which is conducive to the stability and enrichment of fluorine. Br-Cl ratios can be used to analyze the source of salinity in groundwater [30]. As shown in Figure 4, Br-Cl ratios of the geothermal water collected in inland areas (HH05, HH06, HH07, HH08, GH03, GH04, GH05, GH06, and GH07) are less than the ratio of seawater (3.47×10^{-3}), indicating the salinity may come from evaporative halite filtration. Br-Cl ratios of all the cold groundwater and coastal geothermal water exceed the ratio of seawater (3.47×10^{-3}), indicating the salinity of these water samples comes from seawater or marine formation water.

5.2. Isotopic Characteristics of the Geothermal Waters

5.2.1. $^{87}Sr/^{86}Sr$ Isotopes. Relations between $^{87}Sr/^{86}Sr$ and Na of thermal water in the study area, and the isotope references for rocks and mantle are cited from [31–34] (Figure 6). Generally, the older the rock is, the higher the $^{87}Sr/^{86}Sr$ ratio is. The groundwaters have different $^{87}Sr/^{86}Sr$ ratios after interacting with different rock minerals. When geothermal water flows through different minerals in the long-term underground circulation process, a series of reactions occur in the minerals to make the geothermal water have similar $^{87}Sr/^{86}Sr$ ratios with the rock minerals [31]. Therefore, $^{87}Sr/^{86}Sr$ ratio is often used to indicate the degree of water-rock interactions of geothermal waters, source of thermal waters, and mixing of different water bodies. In addition, by the quick assimilation with host rock, the fluid $^{87}Sr/^{86}Sr$ ratios are mainly controlled by the mineral type of rocks and ion exchange with minerals, which makes it an idea tool to forecast host rocks [34, 35].

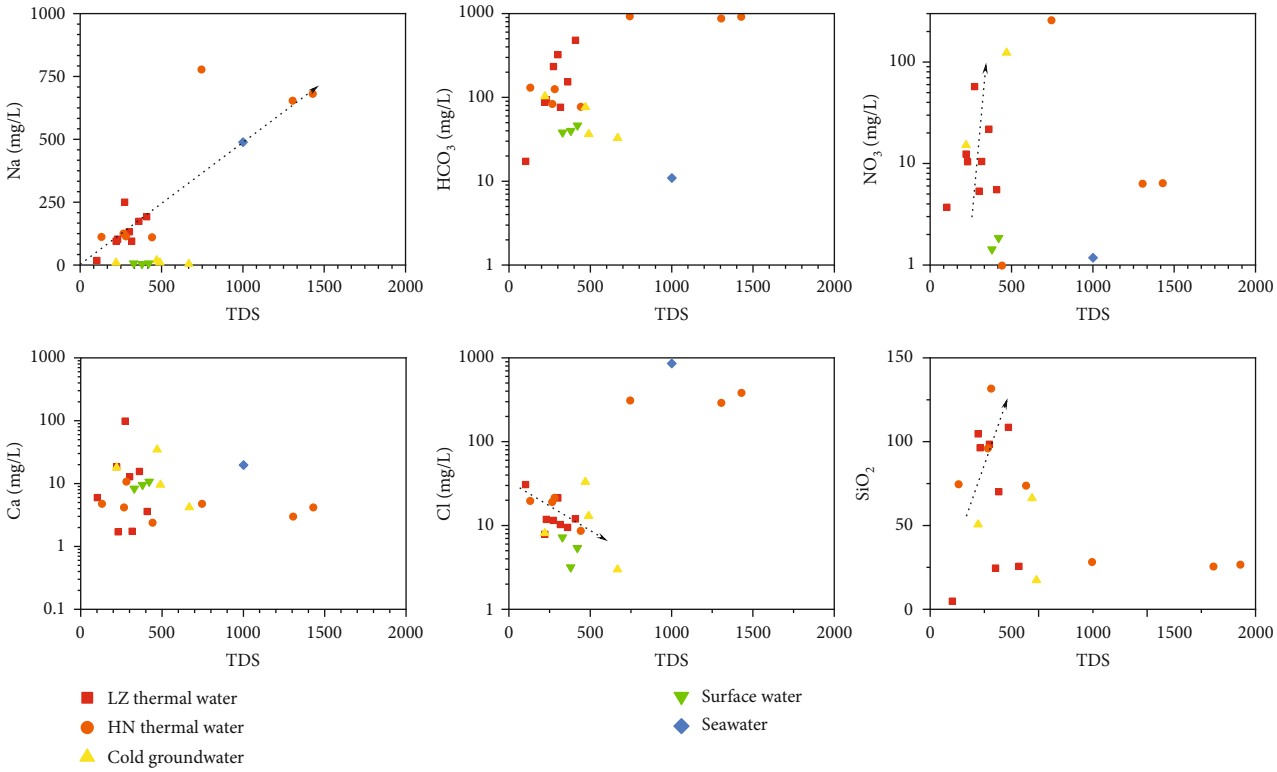

Figure 4: Relationships between various ions (NO_3, Na, Ca, Cl, HCO_3, and SiO_2) and TDS for LZ and HN thermal and cold waters.

The $^{87}Sr/^{86}Sr$ ratios of the Group 1 water samples in north of LZ are significantly greater than other water samples and close to the Paleozoic granite line, especially GH05 and GH07 water samples (Figure 6). The caprocks in LZ inland area are dominated by Paleozoic granite, clastic rock, and argillaceous rock, which results in a similarly high $^{87}Sr/^{86}Sr$ ratios for geothermal water in the area. The $^{87}Sr/^{86}Sr$ ratios of the Group 3 geothermal water are between 0.7100 and 0.7150 and is close to the Mesozoic sedimentary rocks and granites line (Figure 6). The exposed surface strata are dominated by Cenozoic volcanic rocks ($^{87}Sr/^{86}Sr$ ratios from 0.7032 to 0.7085 [33]), but interaction with Cenozoic minerals alone cannot explain the $^{87}Sr/^{86}Sr$ ratio of the Group 2 water samples. Therefore, we speculate that the circulation depth of the geothermal water in this area is greater than the thickness of the basalt, and the geothermal water can interact with older rocks.

It is worth noting that $^{87}Sr/^{86}Sr$ ratios of the Group 2 water samples showed a particularly low $^{87}Sr/^{86}Sr$ ratio (Figure 6). According to the geological condition, the surface water and shallow groundwater are subjected to leaching and ion exchange by Mesozoic basalt and Quaternary sandstone during groundwater circulations. However, the ratio of the Group 2 water samples is slightly lower than the Cenozoic volcanic rocks line and approaches to the mantle line, indicating that the formation of the Group 2 water samples is also affected by other processes. There may be two reasons for the low $^{87}Sr/^{86}Sr$ ratio: (1) It may be that water flows through basalt with a slight mantle origin, which leads to a low $^{87}Sr/^{86}Sr$ ratio. Sun [20] indicated that the basalt magma directly came from the upper mantle in the study area and was not affected by obvious crustal action during the ascent. (2) The extensional structure Wangwu-Wenjiao fault can provide high-quality preferential water channels for the water circulation process, and the water exposed to the ground surface after deep circulation may have a mantle source. Therefore, the mixture of water exposed on the surface and atmospheric precipitation results in a low $^{87}Sr/^{86}Sr$ ratio. Deep geothermal heat source has been suspected to have intruded upward and led to intensified thermal activities. The mantle source of geothermal water may have affected the characteristics of the geothermal water in the tensile tectonic region.

5.2.2. $\delta^{18}O$ and $\delta^{2}H$ Isotopes. Stable hydrogen and oxygen isotopes are important tracers for groundwater studies, which provide pivotal information on water origin, recharge and migration pathways, and fracture permeability to fluids [36, 37]. In addition, δ^2H and $\delta^{18}O$ isotopes are often used to judge among atmosphere, marine, and magmatic origins of hot spring waters. The stable isotope compositions of the thermal waters, cold groundwater, surface water, and seawater are shown in Figure 7, together with the global meteoric water line (δ 2H-δ18O plot for all hot spring samples with the GMWL and LMWL at LZ and HN) [38] and the local meteoric water line (LMWL). The local atmospheric rainfall line includes the LMWL1 in LZ ($\delta^2H = 7.05\delta^{18}O + 6.18$) [15] and LMWL2 in HN ($\delta^2H = 6.77\delta^{18}O - 9.04$) [17]. According to the δ^2H–$\delta^{18}O$ graph, the data points of the thermal water samples in LZ lie close to the GMWL line and the LMWL1 line, indicating there are no signs of an "oxygen shift" from the LMWL1 and GMWL

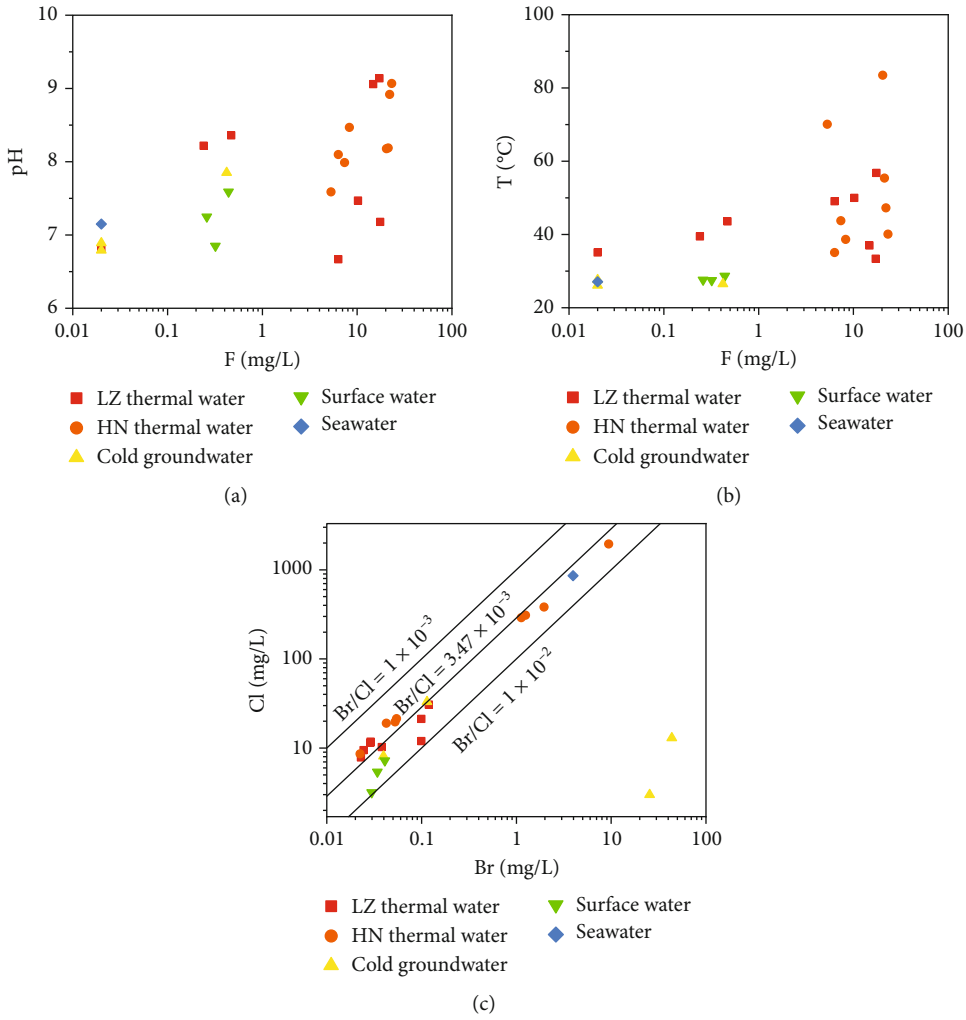

Figure 5: Correlations between F and TDS (a), F and T (b), and Br and Cl(c) for the water samples from LZ and HN areas.

for hot spring waters. The phenomenon shows that the geothermal water is directly derived from atmospheric precipitation. The data points of the geothermal waters in HN deviate from the GMWL and LMWL2 line, indicating a slight positive oxygen "isotope shift" (Figure 7), which results from slight mixing with surface water and cold groundwater. On the one hand, the surface waters have been affected by strong evaporation, resulting in increased δ^2H and δ^{18}O. On the other hand, when the geothermal water rises along the fault to the surface, between oxygen-containing minerals and groundwater occurred isotopic exchange reaction, resulting in the consumption of δ^{18}O isotope [39, 40]. The amount of δ^{18}O isotopic exchange depends strongly on the reservoir temperature, reaction time, and rock compositions. Thus, the range in δ^{18}O isotope content reflects the initial composition of the geothermal water before mixing and the impact of the mixing with shallow cold water. There is an interesting phenomenon that HH03, HH05, and HH07 water samples have oxygen drift, but previous studies have shown that this process is suitable for low-temperature geothermal waters [41]. The temperature of these three water samples exceeds 55°C. Therefore, the above process cannot be used to explain whether the water samples have oxygen drift or not, which will continue to be explored in future studies. As part of the global water circulation, groundwater is in a state of constant renewal, so the renewal ability of groundwater can be used as an important indicator of the process of groundwater circulation [42].

In order to evaluate the renewal ability of geothermal water and supply source, deuterium excess parameter (d) is introduced to measure the δ^{18}O exchange degree in the water-rock reaction. The formula proposed by Dansgaard is $d = \delta^2\text{H} - 8\delta^{18}\text{O}$ [43]. The smaller the value of d, the more closed the hydrogeological environment, the slower the speed of groundwater flow, and the weaker the renewal ability of groundwater [44]. The d value of geothermal water in the study area is between 1.04‰ and 10.78‰, with an average value of 6.83‰, indicating that the hot water is formed by atmospheric precipitation in the current climate (Table 2). Except for GH01, the d value of the hot water samples of the Leizhou Peninsula is close to the d value of the atmospheric rainfall curve, indicating that the water-rock interaction of the hot water after the recharge of atmospheric precipitation is weak, and the groundwater has stronger renewal ability. The overall geothermal water

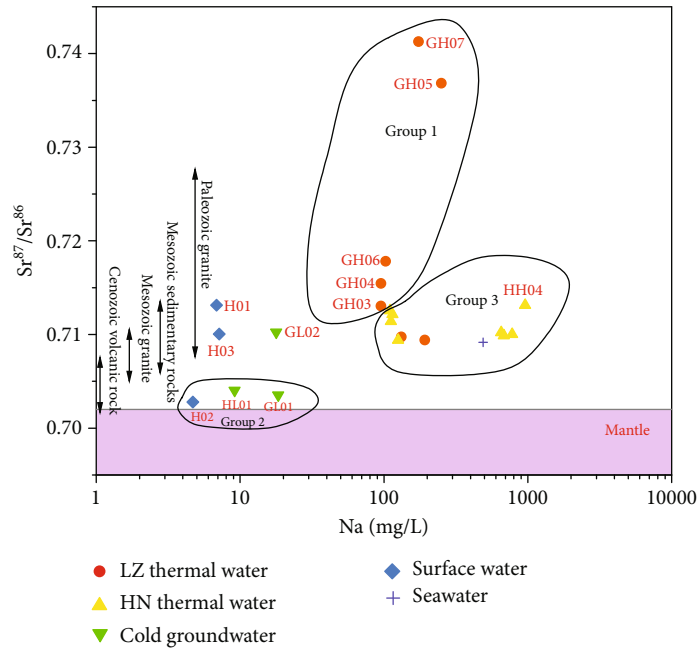

FIGURE 6: Relations between $^{87}Sr/^{86}Sr$ and Na of thermal water in the study area, and the isotope references for rocks and mantle are cited from [31–34].

samples in HN are lower in the d values than those of atmospheric precipitation, which may be the result of "negative drift". Because the H content of atmospheric precipitation is higher than the surrounding rock, it greatly reduced after flowing through the surrounding rocks. Comparing the d values in both LZ and HN, we can find that most hot springs in HN have longer recharge paths, stronger water-rock interactions, and thus stronger renewal ability.

Based upon the δ^2H and $\delta^{18}O$ values of the geothermal waters, the recharge altitude is calculated and used to identify groundwater recharge area. The recharge altitude of groundwater can be calculated as follows:

$$H = H_0 + \frac{\delta_R - \delta_P}{k}. \quad (1)$$

where H is the recharge elevation (m), H_0 is the reference point's elevation, δ_R is the δ^2H or $\delta^{18}O$ value of water samples, δ_P is the δ^2H or $\delta^{18}O$ value of recharge water, and k is the δ^2H or $\delta^{18}O$ elevation gradient of atmospheric precipitation (δ/100 m). Surface water and groundwater are recharged by atmospheric precipitation and shallow groundwater, respectively, which can represent the average annual values of isotope compositions in atmospheric precipitations. Therefore, the average δ^2H value (-40.8‰) of the surface water and cold groundwater samples (H01, H02, H03, HL01, HL02, HL03, and GL01) is identified as δp and the k value is -2‰/100 m, and the H_0 values used in the calculation is obtained from local topographic map. The calculated recharge elevations of the hot springs in the study area are shown in Table 2. The recharge elevation of the study area is ranging from 0.1 m to1430.3 m, with an average of 417.3 m. Based on the local topography and geomorphology, the recharge area of geothermal water in HN includes Wuzhi Mountain (1867 m) and nearby volcanic rock hills. Atmospheric precipitation or bedrock fracture water in mountainous areas replenishes the geothermal water in the study area along water channels such as rock fracture zones and fault zones. The geothermal water samples in LZ have low recharge elevations, and there are mainly two situations, including direct recharge of atmospheric precipitation and indirect recharge through basalt terraces in the southern and northern Leizhou Peninsula.

5.3. Estimation of Temperature and Circulation Depth for Thermal Groundwater

5.3.1. Silicon Geothermometers. Quite a few geothermometers have been proposed in previous studies, but the accuracy of the calculation results depends on actual situations. The application of geothermometers is affected by various factors, including the existence of chemical equilibrium between fluid and minerals during circulation of geothermal waters, reequilibrium from the effect of rising to the surface or from mixing of geothermal waters, and the presence of adequate amounts of the chemical species involved. The application of chemical geothermometers is mainly for high-temperature geothermal systems, which have its share of controversies about the medium- and low-temperature reservoirs [45]. In addition, when the thermal water rises to the surface, the hydrogeochemical information of the geothermal water related to the deep hydrothermal fluid will be partially missing [46, 47]. Therefore, several geothermometer methods need to be compared with each other to determine the temperature of the reservoir. Strict attention should be paid to the assumed conditions that the

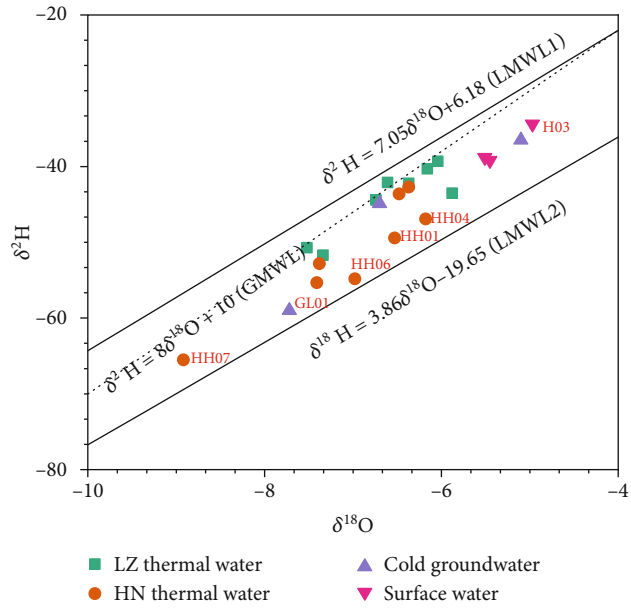

Figure 7: δ^2H-δ^{18}O plot for all hot spring samples with the GMWL and LMWL at LZ and HN.

Table 2: Calculated reservoir temperature (°C), deuterium excess parameter (‰), recharge altitude (m), and reservoir depth (km) for thermal waters.

Sample	temperature	T_1	T_2	T_3	T_4	T_5	T_6	T_7	T_8	T_9	T_{10}	The "FixAl"method	Recharge altitude (m)	Reservoir depth (km)	d (‰)
GH01	43.6	94.4	77.4	23.4	44.4	23.4	-21.4	104.6	21.0	-225.1	82.0	65.0	495.6	1439	9.46
GH02	39.5	92.7	76.0	21.9	42.8	21.9	-22.8	142.8	29.0	-223.3	72.6	76.0	553.7	1802	7.02
GH03	56.8	165.3	134.9	89.1	111.6	89.1	40.5	152.7	28.7	-220.7	97.8	108.0	11.4	2858	8.98
GH04	37	142.5	116.7	67.7	89.8	67.7	20.0	108.9	20.3	-225.1	77.6	110.0	100.3	2924	10.78
GH05	49.1	161.6	132.0	85.7	108.1	85.7	37.2	217.4	52.3	-217.7	88.3	125.0	232.2	3419	9.52
GH06	33.4	160.4	131.0	84.5	106.9	84.5	36.0	135.1	32.1	-221.7	99.8	110.0	0.1	2924	9.02
GH07	50	167.5	136.6	91.2	113.7	91.2	42.5	141.2	29.8	-221.1	102.5	104.0	162.1	2726	8.76
HH01	35.1	98.5	80.8	27.2	48.3	27.2	-17.9	59.1	7.9	-228.9	74.4	86.0	443.4	2132	2.84
HH02	43.8	96.2	78.9	25.0	46.1	25.0	-19.9	70.8	13.6	-228.1	73.2	88.0	144.2	2198	8.24
HH03	38.7	94.3	77.3	23.3	44.3	23.3	-21.4	64.2	11.1	-228.4	76.7	86.0	111.1	2132	8.26
HH04	70.1	166.6	135.9	90.4	112.9	90.4	41.7	183.6	48.0	-208.1	248.0	132.0	315.2	3650	2.54
HH05	47.3	160.2	130.8	84.3	106.7	84.3	35.9	119.9	23.8	-221.1	124.4	88.0	669.1	2198	6.24
HH06	83.5	179.6	146.1	102.7	125.4	102.7	53.6	164.1	36.7	-221.4	80.6	89.0	880.1	2231	1.04
HH07	40.1	145.3	118.9	70.3	92.4	70.3	22.5	116.9	23.7	-224.8	74.3	102.0	1340.3	2660	5.86
HH08	55.4	145.9	119.4	70.8	93.0	70.8	23.0	126.0	24.9	-224.6	70.3	76.0	798.4	1802	3.98

application of chemical geothermometers must be satisfied for every thermal water sample.

In our study, chemical geothermometers are used to estimate geothermal reservoir temperature under different conditions, and their results are given in Table 2. Following are the formulas used:

Quartz no steam loss [49]:

$$T_1 = \frac{1000}{4.78 - \log S}. \quad (2)$$

Quartz with maximum steam loss [49]:

$$T_2 = \frac{1112}{4,91 - \log S} - 273.15. \quad (3)$$

Chalcedony [48]:

$$T_3 = \frac{1390}{5.19 - \log S} - 273.15. \quad (4)$$

Chalcedony with maximum steam loss [48]:

$$T_4 = \frac{1522}{5.75 - \log S} - 273.15. \quad (5)$$

α-cristobalite [49]:

$$T_5 = \frac{1000}{4.78 - \log S} - 273.15. \quad (6)$$

β-cristobalite [49]:

$$T_6 = \frac{781}{4.51 - \log S} - 273.15. \quad (7)$$

Na-K [50]:

$$T_7 = \frac{1217}{\log (Na/K) + 1.483} - 273.15. \quad (8)$$

Na-K-Ca [51]:

$$T_8 = \frac{1647}{\left(\log (CNa/CK) + \beta \log \left(CNa^{0.5}/CK\right) + 2.06\right) + 2.47} - 273.15. \quad (9)$$

Na-K-Mg [52]:

$$T_9 = \frac{1140}{6 \log (Na/K) + \log \left(Mg/Na^2\right) + 18.3} - 273.15. \quad (10)$$

K-Mg [53]:

$$T_{10} = \frac{4410}{13.95 - \log \left(K^2/Mg\right)} - 273.15. \quad (11)$$

The calculation results of various silicon geothermometers are as follows: (1) chalcedony [48] and chalcedony with maximum steam loss [48] yielded temperatures ranging from 23.4°C to 102°C and 42.8°C to 125.4°C, respectively; (2) quartz with no steam loss [49] and quartz with maximum steam loss [49] resulted in temperatures ranging from 92.7°C to 179.5°C and 77.3°C to 146.1°C, respectively; and (3) the temperatures calculated for α-cristobalite [50] and β-cristobalite [50] varying from 21.9°C to 102.7°C and -22.8°C to 53.6°C, respectively.

The mineral saturation index (SI) is very important for the analysis of the applicability of the silica temperature scale, and the SI of the main minerals is shown in Figure 8. The silica geothermometer estimates the thermal reservoir temperature based on the solubility of siliceous minerals (quartz, chalcedony, and cristobalite), which is controlled by the pressure and temperature [54]. The SiO_2 concentration of geothermal waters is directly proportional to the reservoir temperature in general [55]. The shallow groundwater in the study area is mixed with the thermal water exposed on the surface, which leads to a decrease in the SiO_2 concentration. Therefore, the temperatures calculated with SiO_2 geothermometers are often regarded as the minimum reservoir temperatures. Comparing these three silicon geothermometers can draw the following conclusions: (1) It is obviously inaccurate that the calculated temperatures based on β-cristobalite and α-cristobalite geothermometers are less than the temperatures of the springs. (2) In general, at temperatures of less than 180°C, the solubility of silica is usually controlled by chalcedony rather than quartz. However, half of the reservoir temperatures calculated with the chalcedony geothermometer are lower than or close to the geothermal water sample temperature. Therefore, the quart geothermometer was adopted in this article. (3) There is an important reason that the values of the emerging temperatures in the study area are lower than the local boiling point. Therefore, the results estimated with the quart geothermometer without steam loss are relatively more reliable.

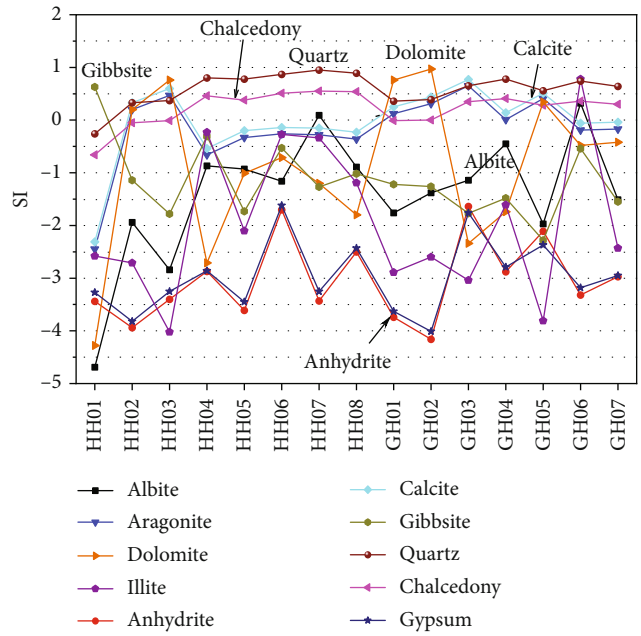

Figure 8: Saturation indices (SI) of the main minerals for the hot springs in study area.

5.3.2. Cation Geothermometers. Another method to estimate thermal water temperature is the use of geothermometers that are based on relationships among cations. When the geothermal water is in equilibrium or at least partially in equilibrium, the geothermometers will consider the cation exchange reaction (Na, K, Ca, Mg, and minerals). This shows that when the thermal water is not in equilibrium, the application of geothermometers will be extremely restricted. Na–K–Mg ternary diagram shows that the water sample HH04 is mature water, and the water samples of HN fall in the area of partially immature waters more than LZ, indicating that interaction between water and rock was more adequate in HN (Figure 9).

Temperatures calculated by Na-K geothermometers are in range from 104.6°C to 217.4°C for LZ and from 59.1°C

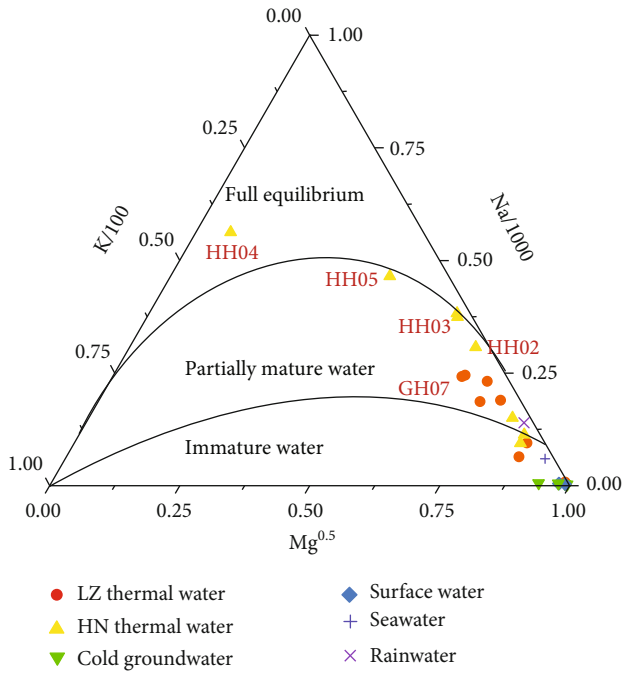

Figure 9: Giggenbach diagram showing relative Na/1000, K/100, and $Mg^{1/2}$ contents (mg/L) based on the water samples from the LZ and HN.

to 164.1°C for HN. It is important to mention that the Na-K geothermometer [50] is mainly recommended for hot springs whose temperature is higher than 180°C, although it has been used in some low-temperature reservoirs that have fluids with long residence times [56, 57]. In general, the Na-K geothermometer relies on the Na/K ratios controlled by the dissolution equilibrium between albite and K-feldspar minerals in geothermal system. Under low temperature conditions, the Na/K ratio is generally not controlled by the cation exchange reaction between the symbiotic alkaline feldspars, and both albite and K-feldspars are difficult to reach equilibrium, which leads to the deviation of the Na-K geothermometer in the medium-low geothermal system. The Na-K geothermometer is not applicable to all hot springs in the study area, and some hot springs are overestimated, especially in LZ.

In order to eliminate the effects of Ca contents on the Na-K geothermometer, the Na-K-Ca geothermometer [51] was used to estimate the temperature. The Na–K–Ca geothermometer is based on the reaction of calcium aluminosilicate to calcite and the equilibrium between Na–K feldspar, which is mainly applied for thermal waters with high calcium concentrations. Ca contents of thermal waters are 1.71–98.66 mg/L and 2.39–293.42 mg/L in the LZ and HN, respectively, and these are not thermal waters with high calcium concentrations. A plausible reservoir temperature estimate in the range from 20.3°C to 52.3°C for LZ and from 7.9°C to 48.0°C for HN can be obtained from Na-K-Ca geothermometer. This geothermometer can calculate the thermal reserve temperature of low-temperature geothermal fields. However, the Ca/Na ratio in the geothermal water is significantly affected by the precipitation of carbonate rock minerals, the dissolution of gypsum minerals, and the precipitation of calcite caused by boiling. The calculated temperatures are lower than the measured field temperatures in this study, which are deemed unreliable. Na-K-Mg geothermometers give unexpectedly low temperatures ranging from -225.1°C to -217.7°C for LZ and from -228.9°C to 208.1°C for HN, which is obviously unreasonable for the natural conditions. K-Mg geothermometer is often used in low-temperature systems, where dissolved Na and Ca have not reached rock–fluid equilibrium [53]. When the temperature changes, this geothermometer readjusts relative content in mixing systems in a way faster than Na-K geothermometer, which represents rapid reequilibrium occurs in the shallow hot water reservoir. Temperature estimated by K-Mg geothermometer ranges from 77.6°C to 102.5°C for LZ and from 70.3°C to 248.0°C for HN. There still exists an important phenomenon that half of the geothermal waters is partially mature water in the study area, which reflect some level of uncertainty regarding the mineral compositions, whether the equilibrium minerals related to the traditional geothermometers in the low-medium and high temperature reservoirs [57]. Therefore, the Na-K and K-Mg geothermometer may have a certain deviation, but they can be compared and referenced with each other.

5.3.3. Multimineral Geothermometers. Precise prediction of reservoir temperature can be achieved by using the saturation indexes (SI) of multimineral at different temperatures. It includes simulating the gradual increase in the temperature of the hydrothermal fluid and observing the changes in different saturation states assumed minerals present in the equilibrium conditions of the reservoir. To achieve this, the SI of multiple minerals presumably present in the reservoir are calculated at the specified temperatures ranging between 25°C and 175°C by using the computer program PHREEQC. It is necessary to keep in mind that geothermal water incurs loss of CO_2 near the surface, which affects pH and the calculation of mineral saturation. In order to eliminate the influence of the loss of CO_2, the CO_2 in the geothermal water is replaced until the calcite reaches equilibrium [58].

Meanwhile, Al content in the geothermal system is low and difficult to accurately measure, and the lack of Al in geothermal water can easily plot a wrong Q/K diagram. The "FixAl" method was used to alleviate the problem associated with lack of Al determination in many chemical analyses and requires to force the water to be at equilibrium with selected Al-bearing minerals [59]. The Al content in the geothermal water in the study area is assumed to be 0.3 mg/L, and the contents of the rest of the components are multiplied by appropriate coefficients (GH01 × 2.5, GH02 × 2.6, GH03 × 2.5, GH04 × 1.2, GH05 × 2.6, GH06 × 2.4, GH07 × 4.5, HH04 × 3.0, HH02 × 3.2, HH03 × 3.1, HH04 × 2.5, HH05 × 1.0, HH06 × 1.1, HH07 × 1.1, and HH08 × 1.0). In the Q/K diagram, when the curves of multiple minerals converge to a point, the convergence point of the simulated aluminosilicate minerals is the most likely equilibrium temperature value. If multiple minerals in geothermal water are close to equilibrium at a certain temperature, this temperature is the thermal reservoir temperature (Figure 10).

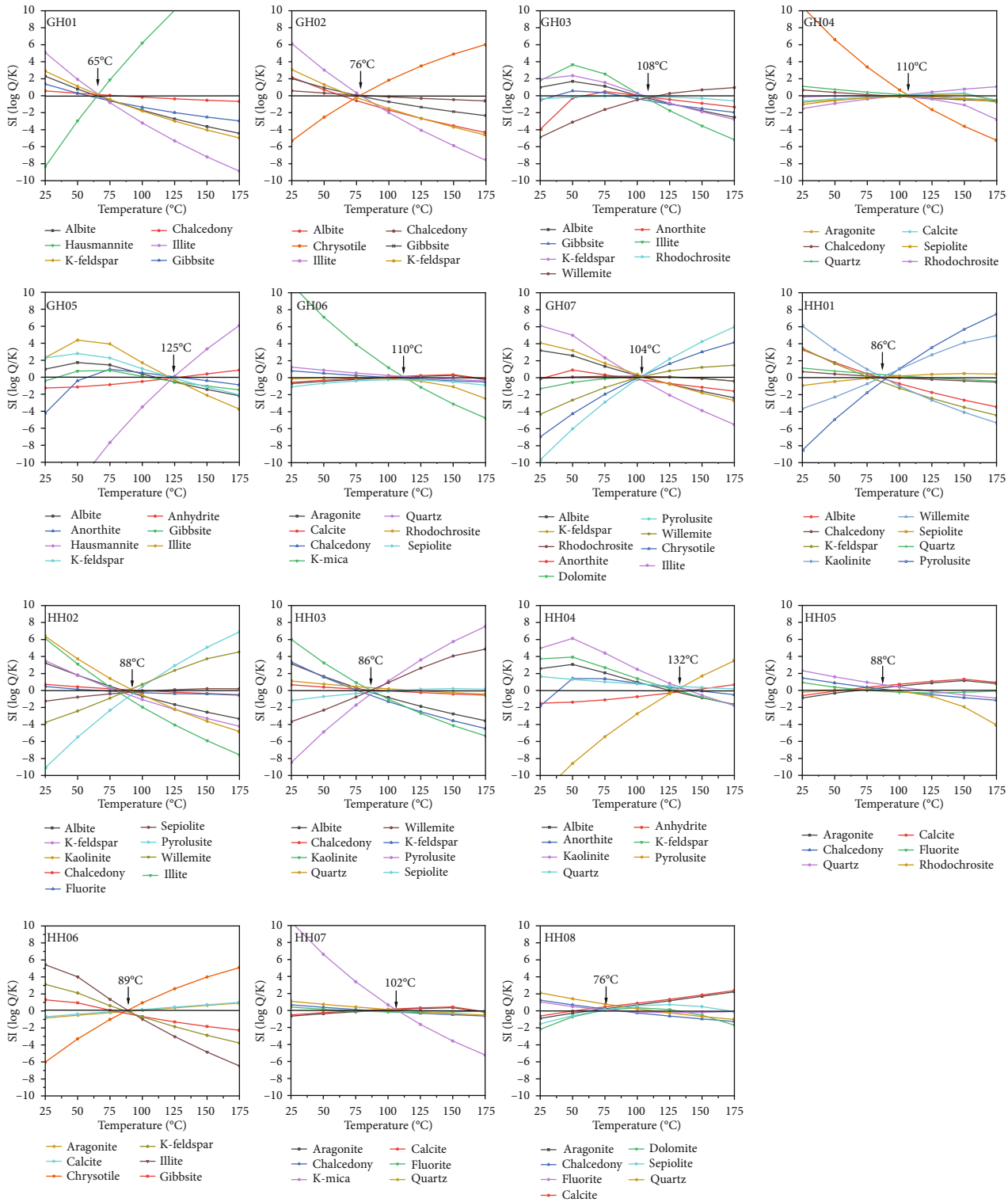

Figure 10: Fixed-Al mineral equilibrium diagrams showing the hot spring water samples in study area.

The simulation results show that the reservoir temperature of the geothermal water in HN is between 65°C and 132°C, and the main minerals in the equilibrium state include albite, K-feldspar, calcite, chalcedony, and anhydrite. For the HN hot springs, saturation indices with respect to calcite, chalcedony, quartz, anhydrite, and other minerals converge to the zero line at temperatures of 100°C–165°C, at which temperature range these minerals are assumed to be in equilibrium with water giving rise to the estimated reservoir temperature (Figure 10). Multicomponent mineral

equilibrium temperature for fifteen thermal water samples is shown in Figure 10, which is also consistent with the values (76.0°C–146.1°C) obtained by quart geothermometer without steam loss.

5.3.4. Circulation Depth. Hot springs are generally formed when shallow groundwater flows toward regional discharge area and is heated by the crustal thermal flow before exposed in the surface, which means that the temperature of the hot springs is provided by geothermal heating. The correlation between the circulation depth of hot water and thermal reservoir temperature can be used to roughly calculate the circulation depth of geothermal water. The calculation formula of geothermal water circulation depth can be estimated as follows:

$$D = G(T - T_0) + Z_0, \tag{12}$$

where D is the fluid circulation maximum depth (m); T_0 is the local annual temperature (°C); G is the geothermal level (reciprocal of the geothermal gradient); T is the estimated reservoir equilibrium temperature (°C), and Z_0 is the thickness of the constant temperature zone (m). Below the constant temperature zone, the temperature changes continuously with depth, forming a geothermal gradient. Hot springs are mainly exposed in granite and basalt formations, T_0 and Z_0 is 22°C and 20 m, respectively. G refers to the incremental rate of the temperature with depth of the crustal strata without being affected by atmospheric temperature. The G calculated using Huadong borehole data in 2018 is 26.70 m/°C (Figure 1. d; Prof. LI Dewei, personal communication, 2018). The geothermal gradient increment signifying intense geothermal activities, and the temperature and thermal outflux of the deep heat source are relatively high. The "Heat Flow Data in Mainland China" proposed by Jiang et al. [60] shows that the range of the geothermal gradient in the study area is 24.04 m/°C to 46.73 m/°C, and the average value is 31.75. There is a limited variation in the range of the gradient value, indicating that the geothermal gradient calculated based on the Huadong borehole can be used as the geothermal gradient in the study area. The circulation depth of the study area ranges from 1168 to 2957 m, and the average circulation depth is 2023 m. The calculated shallow circulation depth is consistent with the shallow circulation characteristics proposed by Gao et al. [61].

Regarding geothermal reservoir, it is noteworthy that reservoir concept is relative to the circulation of the water of interest. The Huadong deep borehole at 4387-m-depth is still within the Jurassic sandstone formation, failing to reach the formation bottom boundary interface. The unconformity interface between Cretaceous and Jurassic formations could serve as a preferential path for the geothermal waters. This unconformity interface is a geothermal reservoir yet untapped. Current geothermal spring data could not provide more information regarding this unconformity reservoir. Exploration deep enough to capitalize the thermal resources should key in on reaching breakthrough of the conformity boundary interface of the sandstones.

5.4. Inverse Modeling of the Hot Springs

5.4.1. Simulation Basic Theory. Hydrogeochemical simulation is an important means to study the changes of groundwater chemical compositions and the evolution during the cycle. Through simulation calculations, the existence of groundwater chemical components can be quantitatively studied and the hydrogeochemical reactions occurring in the circulation process can be clarified. In the process of hydrothermal circulations of different hot springs, the circulation depth, main minerals, and circulation paths affected by the fault are different, resulting in great differences in the mineral dissolution reactions. Thus, it is necessary to understand quantitatively the mineral phases involved in chemical reactions during geothermal water circulations along the flow path.

In this paper, the reverse simulation of PHREEQC software is used to identify the evolution of ions in water-rock interactions, which provide support for the quantitative study of ion migrations in the process of geothermal water circulation [62]. The procedure of selecting reactants is essential to establish the reverse reaction model, based on minerals of the aquifer and chemical compositions of groundwater and occurrence conditions of groundwater. The lithology of the stratigraphic rocks in the study area is mainly basalt, granite, magmatic granitoid, clay, and sandstones. The main minerals of the rocks are albite, quartz, calcite, dolomite, anorthite, and fluorite. The hot spring is in an open system, and CO_2 should be considered as possible mineral. Since the study area belongs to the coastal area, the salinity of the seawater gradually accumulates on the surface to form a halite layer; therefore, salt rock is considered as possible mineral [63]. In summary, possible minerals finally selected include albite, anorthite, gypsum, halite, calcite, dolomite, quartz, CO_2, fluorite, NaX, CaX_2, and KX. The selection of constrained variables is determined by changes of various chemical components in the process of geothermal water circulation. A total of 9 chemical elements (K, Ca, Na, Mg, Cl, SO_4, HCO_3, F, and SiO_2) are determined as constraint variables of reaction simulations in mass balance. Mass balance simulation model is the basis of reverse simulation, which calculates the molar transfer of chemical elements into the groundwater and deduces the possible geochemical interactions between the paths based on the chemical composition of the water at origin and destination. The formula is as follows:

$$\begin{aligned}\sum_{n=1}^{P} a_n b_{n,k} &= m_{T,k}(\text{origin}) - m_{T,k}(\text{destination}) \\ &= \Delta m_{T,k}\, k = 1, 2 \cdots j,\end{aligned} \tag{13}$$

where a_n represents the change of the amount molar of mineral n entering (positive value) or leaving (negative value) geothermal water; $b_{n,k}$ stands for the stoichiometric number of element k in mineral n (i.e., that the molar amount released after 1 mol of mineral n is completely dissolved); $m_{T,k}$ (origin) and $m_{T,k}$(destination) is the total mass molar concentration of element k in groundwater; j represents

the number of all elements in the calculation; and $\Delta m_{T,k}$ means the change of the total molar concentration of a certain element k between origin and destination of the geothermal water cycle caused by the mineral dissolution, precipitation, and gas migration.

5.4.2. Simulation Path. According to the geological characteristics and topography, the geothermal anomaly area with dense hot spring distribution and high exposure temperature is selected for the simulation (Figure 1(a)). The high-altitude hot spring is selected as the starting point of the simulation path, and the low-altitude hot spring is selected as the end point. The path is selected in three typical areas, including both sides of the Qiongzhou Strait, the high-temperature hot spring area in the middle of Hainan Island, and the northern part of Leizhou Peninsula. Route 1 and Route 2 are distributed on both sides of the Qiongzhou Strait, with extensive exposure of basalt. The starting and ending points are HH02 and GH01 and HH01 and GH02, respectively. Route 3 is located in the northern part of Hainan Island, which is typical high-temperature hot springs in the study area, and HH06 and HH08 are chosen as the origin and destination. In order to explore the influence of the Suixi Fault on the hot spring and compare it with the hot spring in the volcanic rock area, GH06 and GH04 are selected as the origin and destination of Route 4, respectively. The formation of geothermal waters involves numerous reactions and complex environments, and the uncertain value is constantly adjusted to minimize the value of the output solution.

5.4.3. Simulation Results. The results of the reverse geochemical simulations are shown in Table 3 and Figure 11. A positive molar transfer number indicates that the mineral dissolved, while a negative number indicates that the mineral precipitated and left the groundwater in the form of ions. Path 1 and Path 2 are located on the respective south and north sides of the Qiongzhou Strait (Figure 1(c)), the temperature of the hot springs is around 40°C, and the molar transfer volume shows a similar trend. During the hydrothermal cycle of Path 1, albite, calcite, and gypsum dissolved, accompanied by strong cation exchange. CO_2 storage increases in the reservoir environment due to the higher pressure and higher reservoir temperature environment. The Na content increased from 681.25 mg/L to 778.12 mg/L, mainly caused by the dissolution of albite and ion exchanges. At the same time, the dissolution of albite is the main source of SiO_2 and K in the shallow circulation. The dissolution of gypsum and calcite contributed to the increase of Ca content from 4.18 mg/L to 4.78 mg/L. The Path 2 is located along the coast of Xuwen County on the Leizhou Peninsula, with a flat terrain. The mineral reactions in the Path 2 hydrothermal cycle are similar to the Path 1, but the degree of reaction is more intense, especially the dissolution reaction of albite (Figure 11).

Path 3 is located between the Wangwu-Wenjiao fault and the Changjiang-Qionghai fault, with the largest circulation depth among the four paths. Both the origin and destination belong to high-temperature hot springs, and especially, the temperature of HH06 hot Spring is as high as 83.50°C, which is the hottest hot spring in the study area. The Path 3 has a low molar transfer rate, indicating that the mineral reaction in the path becomes weaker, as the migration time and depth increase. Along the deep cycle migration Path 3, weak ion exchange and dissolution of calcite and fluorite occurred. Path 4 is located near Zhanjiang in the north of Leizhou Peninsula, adjacent to the Suixi fault. The dissolution reaction of quartz is the dominant reaction, leading to a substantial increase in SiO_2. The content of F increased from 6.33 mg/L to 17.50 mg/L, which was mainly derived from the dissolution of fluorite. Overall, dolomite, quartz, and anorthite are dissolved along the subsurface thermal groundwater flow path, accompanied by strong ion exchanges. The reverse geochemical simulation results reveal that the geological background, hydrogeological conditions, and fractures coordinately control the flow field of the geothermal water and the degree of water-rock interactions. This has certain significance in understanding the chemical evolution mechanism of geothermal water and the dynamic characteristics of geothermal water in the study area.

Table 3: Mole transfers simulated by PHREEQC (mmol/kg).

	HH02 to HH01	HH06 to HH08	GH01 to GH02	GH06 to GH04
Halite	-1.41E-03	-4.97E-05	-2.32E-04	-3.25E-05
Gypsum	8.87E-05	-3.00E-04	2.36E-05	-3.22E-04
Calcite	1.05E-03	7.75E-05	1.41E-03	-1.09E-04
Dolomite	-3.01E-05	-1.52E-05	-4.49E-05	2.88E-06
Fluorite	-2.74E-05	1.79E-05	6.06E-06	-2.13E-05
Albite	2.14E-03	-7.12E-05	3.29E-03	-9.00E-04
CO2(g)	9.08E-04	2.47E-04	1.21E-03	3.11E-05
NaX	2.20E-05	3.47E-05	3.33E-05	3.53E-05
Quartz	-4.25E-03	-8.08E-04	-6.56E-03	1.36E-03
Anorthite	-1.07E-03	3.56E-05	-1.65E-03	4.50E-04
KX	-2.20E-05	-6.93E-05	-3.33E-05	-3.53E-05

5.5. Genesis Analysis of Hot Springs in the Research Area. In the Leizhou Peninsula, the caprock is dominated by Quaternary clay, sandstone, and basalt in southern and is mainly composed of terrigenous polyflysch group in the northern part of the region (Figure 12). The background value of terrestrial heat flow in the study area is 60-70 mW/m^2. Volcanic activities were frequent during the Quaternary, but the temperature of hot springs was low [20, 60]. Therefore, the heat source is dominated by deep geothermal flow, supplemented by magma residual heat. Hydrogen and oxygen isotopes indicate that the geothermal waters of Leizhou Peninsula originate from the modern atmospheric precipitation, which enters the groundwater circulation system along the direction of the fault channel and main fracture zones. Regional faults are well-developed, and the existence of faults represented by the Suixi fault not only provides excellent water flow channel for the deep circulation of hot springs but also the intersecting tensile and shear geostructures makes it easier for the rising hot water to be exposed to the surface. The

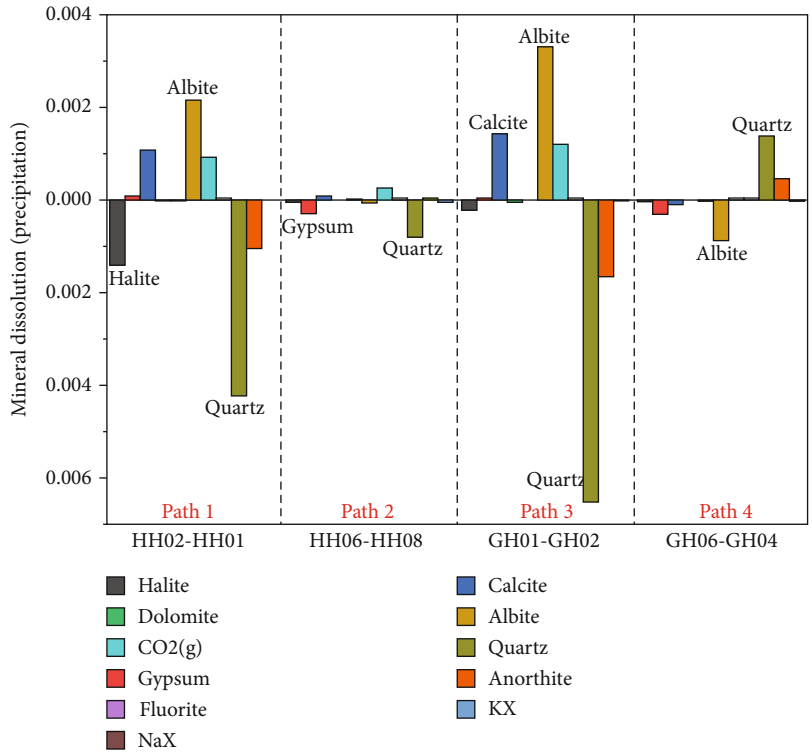

FIGURE 11: Mole transfer simulations in study area, Path 1 is the simulation from HH02 to the HH01 spring, Path 2 is the simulation from HH06 to the HH08 spring, Path 3 is the simulation from GH01 to the GH02 spring, and Path 4 is simulation from GH06 to the GH04 spring.

deep circulating geothermal water is heated by geothermal heating and deep heat transfer, which is driven by the hydraulic difference and the increase of buoyancy to move upward along the fractures. When the hot water rises along the fault, it experiences shallow underground cold water mixing and seawater intrusion and then emerges near the intersection of tensile and shear geostructures. According to the results of PHREEQC simulations, the hydrothermal circulation process of the volcanic rocks on both sides of the Qiongzhou Strait is similar, but the mineral reactions of Leizhou Peninsula are more intense. Albite, gypsum, and calcite are dissolved, accompanied by strong ion exchange reactions.

The heat source of Hainan Island is similar to that of Leizhou Peninsula, which is dominated by deep thermal flow. The thermal reservoir caprock in Hainan Island is more complex, including Quaternary clay, sandstone, Cenozoic basalt, migmatic granitoid, Jurassic terrigenous clastic rock, and Yanshanian 3rd epoch granite (Figure 12). The caprock directly controls the heat loss during the formation of geothermal waters and provides the basic conditions for the formation of higher temperature geothermal waters. The deuterium excess parameter indicates that the hydrogeological conditions of the caprocks are more closed, and the renewal ability of groundwater is weaker. Hainan Island has a high recharge elevation, a long recharge distance, and a long deep circulation time, resulting in slight "oxygen drift". After atmospheric precipitation falls to the hilly areas formed by volcanic rocks and Wuzhi Mountain, it enters the groundwater circulation system after infiltrating in favorable areas. The geothermal water circulation in Hainan Island is deeper, and the temperature of the thermal reservoir is about 70-160°C. The low $^{87}Sr/^{86}Sr$ ratio of Hainan Island indicates that the water body is likely to have a deep mantle source.

6. Conclusions

We studied the geothermal water systems across the Qiongzhou Strait through the hydrogeochemistry and trace elements and multiple isotopes in hydrogen, oxygen, and strontium. We can find there is no significant difference in the water chemistry and isotopic characteristics of the geothermal waters in the two regions separated by the Qiongzhou Strait. But these characteristics of the thermal waters are distinctively different from those of cold shallow groundwater and surface waters. The water chemical results show that most geothermal waters are nearly alkaline and HCO_3-Na types, while the groundwater samples are significantly different, having HCO_3-Ca, HCO_3-Mg, and HNO_3-Ca types. The geothermal water in the study area is rich in trace elements including B, Li, As, Br, and F. The high content of fluorine mainly comes from fluorite dissolution and precipitation, adsorption and desorption, and cation exchange.

Geothermal waters in the LZ northern area have a similarly high $^{87}Sr/^{86}Sr$ ratios, resulting from the caprocks in the northern LZ is dominated by Paleozoic granite, clastic rock, and argillaceous rock. The $^{87}Sr/^{86}Sr$ ratios of other

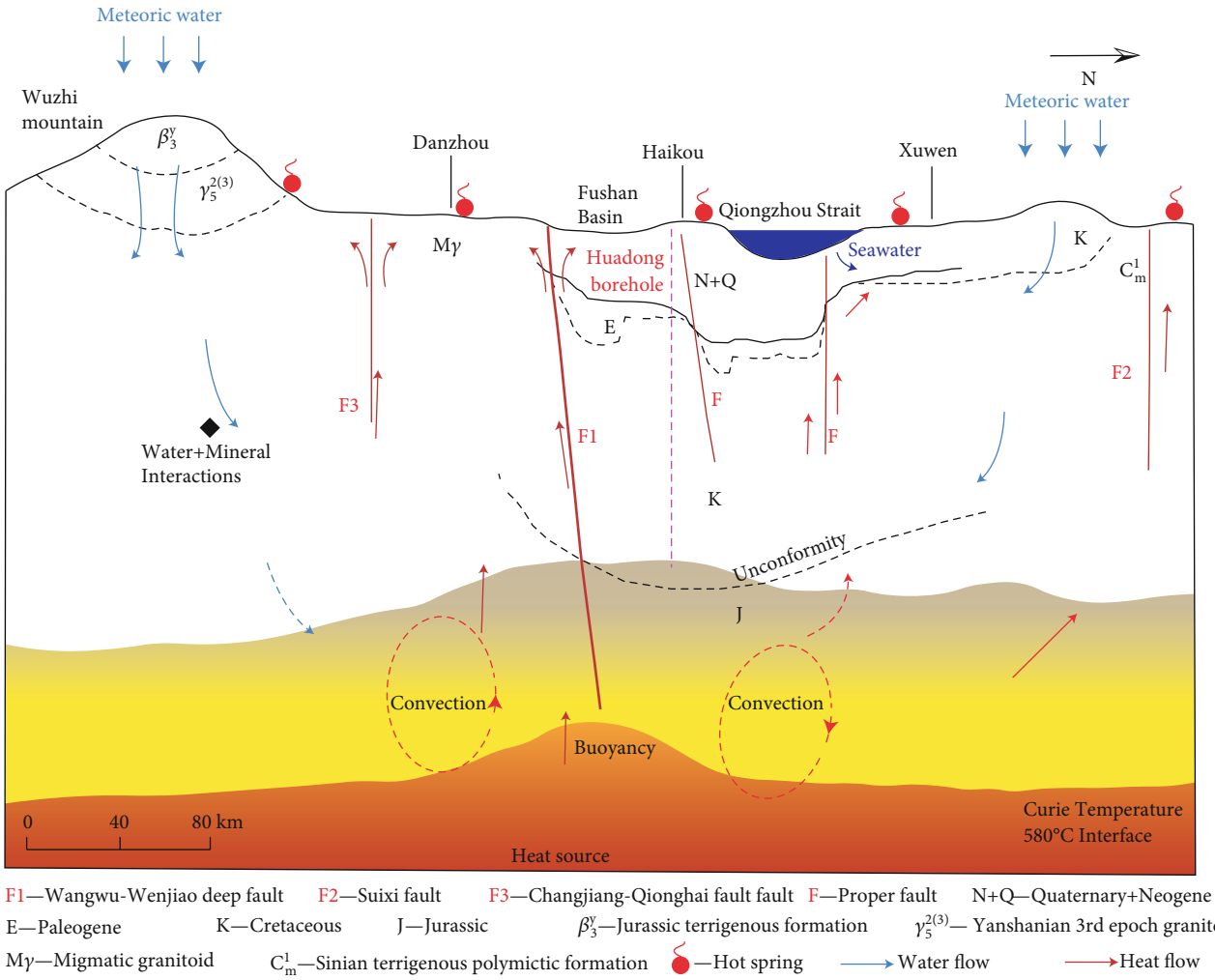

Figure 12: Conceptual model of hydrothermal system in Leizhou Peninsula and Hainan Island in South China.

geothermal waters are relatively low and between 0.7100 and 0.7150, indicating that geothermal water circulates below the Cenozoic basalt layer and reacts with older rocks. The $^{87}Sr/^{86}Sr$ ratios of some groundwater and surface water showed a particularly low $^{87}Sr/^{86}Sr$ ratio in the study area. It could be that water flows through basalts with mantle origin, which leads to a low $^{87}Sr/^{86}Sr$ ratio. The extensional structure Wangwu-Wenjiao fault can provide preferential water channels for the water circulation process, and the water exposed to the ground surface after deep circulation may have a mantle source. The mixture of water exposed on the ground surface and atmospheric precipitation results in a low $^{87}Sr/^{86}Sr$ ratio. Stable isotopes data indicate that the hot springs in LZ are meteoric in origin, while the geothermal water in HN has a slight "oxygen drift," and water-rock interaction and evaporation together lead to the phenomenon of "oxygen drift." Comparing the deuterium excess parameter in both LZ and HN, we can find that most hot springs in HN have longer recharge paths, stronger water-rock interactions, and stronger the renewal ability. The recharge elevation of the study area is ranging from 0.1 m to 1430.3 m, with an average of 417.3 m.

Thermal geothermal waters were qualified as immature and partially mature waters according to Na–K–Mg ternary diagram. Both Na-K-Mg and Na-K-Ca cation geothermometers results were unreliable due to the lack of equilibrium between geofluids and concerned minerals. In contrast, the temperature calculated by the Na-K and K-Mg geothermometers is reliable to certain extent in comparison with observed field temperatures of the outflows and can thus be used as a reference for other geothermometers. Multicomponent mineral equilibrium and quart geothermometer without steam loss successfully predicted the deep reservoir temperature which was estimated to be in a range of 65.0°Cto 165.0°C at average circulation depth of 2023 m. The circulation depths were substantiated by multithousand-meter-deep borehole drilled in the sedimentary basin in northern coast of Hainan Island. According to the results of PHREEQC simulations, the hydrothermal circulation process of the volcanic rocks on both sides of the Qiongzhou Strait is similar, but the mineral reaction of Leizhou Peninsula is more intense. Albite, gypsum, and calcite are dissolved, accompanied by a strong ion exchange reaction. The hot springs in the central part of Hainan Island

belong to high-temperature deep-circulating water, with low molar transfer and low water-rock interaction during the hydrothermal circulation. The main reaction is the precipitation reaction of quartz and gypsum, accompanied by weak ion exchange. The hot springs in the southern Leizhou Peninsula belong to high-alkalinity hot spring water, and the dissolution of quartz and the precipitation of albite are the main controlling reactions of the regional hydrothermal circulation.

Deep geothermal heat source has been suspected to have intruded upward and led to intensified thermal activities. We found that the geothermal gradient increment signifies intense geothermal activities, relatively high temperature, and thermal outflux of the deep heat source. And we also found that the mantle source of geothermal water may have affected the characteristics of the geothermal water in the tensile tectonic region. It is noteworthy that geothermal reservoirs in this study region are largely underlying and trapped by the regional caprocks largely known as the Jurassic sandstone layers.

This paper has discussed the comprehensive use of major elements, trace elements, and multiple isotopes ($^{87}Sr/^{86}Sr$, $\delta^{18}O$, and $\delta^{2}H$), systematically characterizations of the hydrogeochemical evolution characteristics of the study area and quantitatively calculation of the circulation depth and renewable capacity of geothermal water. Difficulty in determining reservoir temperature still has been met as usual for geothermal fields, using methods such as silicon geothermometers, cation geothermometers, and multimineral equilibrium simulation. We provide high end member of thermal gradient, substantiated by the deep borehole data.

Based on the hydrochemical characteristics and evolution of the geothermal waters, the research provided the first insight into the coastal extensional geothermal field and may be useful for researchers in geothermal, hydrogeology, tourism economy, and environment. The results will help to better elucidate the strong hydrothermal activities, abnormal geothermal background, and tectonic evolution of the LZ and HN. Due to the lack of long-term monitoring data, the quantitative research on the evolution mechanism of geothermal water needs to be further explored in the future.

Data Availability

The data used to support the findings of this study are included within the article.

Conflicts of Interest

The authors declare that they have no conflicts of interest.

Acknowledgments

This research project was financially supported by the National Natural Science Foundation of China (Grant number 41572241) and China Postdoc Science Foundation (Grant number 2021 M701411). We express our gratitude for help in our field trips from LUO Shaoyin, LIANG Jie, LIANG Jin, and YU Weidong and inspiration from late beloved Professor LI Dewei (China University of Geosciences (Wuhan)).

References

[1] M. Ta, X. Zhou, J. Guo, Y. Wang, X. Wang, and Y. Xu, "Hydrogeochemical characteristics and formation of the hot springs occurring in the plunging ends of an anticline in Chongqing, Eastern Sichuan Basin, China," *Environmental Earth Sciences*, vol. 78, no. 15, pp. 1–14, 2019.

[2] B. B. Wang, G. P. Lu, X. N. Hu, and H. Ou, "Hydrochemical characterization of thermal spring waters in the deep fault region in western Guangdong," *Environment and Chemistry*, vol. 38, no. 5, pp. 1150–1160, 2019.

[3] X. Wang, G. Lu, and B. X. Hu, "Hydrogeochemical characteristics and geothermometry applications of thermal waters in Coastal Xinzhou and Shenzao geothermal fields, Guangdong, China," *Geofluids*, vol. 2018, 24 pages, 2018.

[4] B. Yan, S. W. Qiu, Z. Liu, and X. Changlai, "Characteristics of the geothermal water in Changbai Mountain volcanic region, northeast of China," *Arabian Journal of Geosciences*, vol. 10, no. 12, pp. 1–13, 2017.

[5] M. L. Liu, Y. W. Cao, M. D. Wang, J. X. Li, and Q. H. Guo, "Source of hydrochemical composition and formation mechanism of Rehai geothermal water in Tengchong," *Safety and Environmental Engineering*, vol. 6, pp. 1–7, 2014.

[6] G. L. Wang, Y. G. Liu, X. Zhu, and W. Zhang, "The status and development trend of geothermal resources in China," *Earth Science Frontiers*, vol. 27, no. 1, p. 1, 2020.

[7] G. L. Wang, W. Zhang, J. Y. Liang, W. J. LIN, Z. M. Liu, and W. L. Wang, "Evaluation of geothermal resources potential in China," *Acta Geoscientica Sinica*, vol. 38, no. 4, pp. 449–459, 2017.

[8] H. Q. Huang, X. H. Li, Z. X. Li, and W. X. Li, "Intraplate crustal remelting as the genesis of Jurassic high-K granites in the coastal region of the Guangdong Province, SE China," *Journal of Asian Earth Sciences*, vol. 74, pp. 280–302, 2013.

[9] G. Zhang, C. Q. Liu, H. Liu, Z. Jin, G. Han, and L. Li, "Geochemistry of the Rehai and Ruidian geothermal waters, Yunnan Province, China," *Geothermics*, vol. 37, no. 1, pp. 73–83, 2008.

[10] H. Song and Z. Zhang, "Evaluation of sustainable tourism development of the hotel industry in Hainan, China by earth check," *Open Access Library Journal*, vol. 1, no. 9, pp. 1–12, 2014.

[11] L. Yan, X. Xie, K. Peng et al., "Sources and compositional characterization of chromophoric dissolved organic matter in a Hainan tropical mangrove-estuary," *Journal of Hydrology*, vol. 600, article 126572, 2021.

[12] Q. Zhang, Z. Tao, Z. Ma et al., "Riverine hydrochemistry and CO2 consumption in the tropic monsoon region: a case study in a granite-hosted basin, Hainan Island, China," *Environmental Earth Sciences*, vol. 75, no. 5, p. 436, 2016.

[13] L. Chen, T. Ma, Y. Du et al., "Hydrochemical and isotopic (^{2}H, ^{18}O and ^{37}Cl) constraints on evolution of geothermal water in coastal plain of Southwestern Guangdong Province, China," *Journal of Volcanology and Geothermal Research*, vol. 318, pp. 45–54, 2016.

[14] X. Zhou, M. Chen, and C. Liang, "Optimal schemes of groundwater exploitation for prevention of seawater intrusion in the

Leizhou Peninsula in southern China," *Environmental Geology*, vol. 43, no. 8, pp. 978–985, 2003.

[15] H. X. Zhang, Y. Wu, W. Y. Luo, W. Chen, and H. Q. Liu, "Hydrogeochemical Investigations of Groundwater in the Lingbei Area, Leizhou Peninsula," *Huan Jing Ke Xue*, vol. 41, no. 11, pp. 4924–4935, 2020.

[16] Y. Lu, C. Tang, J. Chen, and J. Chen, "Groundwater recharge and hydrogeochemical evolution in leizhou peninsula, China," *Journal of Chemistry*, Article ID 427579, 2015.

[17] Z. Ying, "Research on the characteristics and causes of hot springs in Hainan Island," *China University of Geosciences*, 2019.

[18] W. Zhong, J. Cao, J. Xue et al., "Carbon isotope evidence of last glacial climate variations in the tropical NW Leizhou Peninsula, South China," *Boreas*, vol. 41, no. 1, pp. 102–112, 2012.

[19] Z. Zheng and Z. Q. Lei, "A 400,000 year record of vegetational and climatic changes from a volcanic basin, Leizhou Peninsula, southern China," *Palaeogeography, Palaeoclimatology, Palaeoecology*, vol. 145, no. 4, pp. 339–362, 1999.

[20] S. Qian, "Quaternary volcanic activity and magma evolution in north Hainan Island," *China Seismological Bureau*, 2003.

[21] P. Stelling, L. Shevenell, N. Hinz, M. Coolbaugh, G. Melosh, and W. Cumming, "Geothermal systems in volcanic arcs: volcanic characteristics and surface manifestations as indicators of geothermal potential and favorability worldwide," *Journal of Volcanology and Geothermal Research*, vol. 324, pp. 57–72, 2016.

[22] H. Alçiçek, A. Bülbül, and M. C. Alçiçek, "Hydrogeochemistry of the thermal waters from the Yenice Geothermal Field (Denizli Basin, Southwestern Anatolia, Turkey)," *Journal of Volcanology and Geothermal Research*, vol. 309, pp. 118–138, 2016.

[23] W. M. Edmunds and P. L. Smedley, "Residence time indicators in groundwater: the East Midlands Triassic sandstone aquifer," *Applied Geochemistry*, vol. 15, no. 6, pp. 737–752, 2000.

[24] A. A. El-Fiky, "Hydrogeochemistry and geothermometry of thermal groundwater from the gulf of suez region, Egypt," *Earth Sciences*, vol. 20, no. 2, pp. 71–96, 2009.

[25] X. Dan, *Hydrogeochemistry of Geothermal Field of Long Mu Bay*, East China University of Technology, Hainan Province, 2017.

[26] W. Cumming, "Resource conceptual models of volcano-hosted geothermal reservoirs for exploration well targeting and resource capacity assessment: construction, pitfalls and challenges," *Geothermal Resources Council Transactions*, vol. 40, pp. 623–637, 2016.

[27] E. González-Partida, A. Carrillo-Chávez, G. Levresse et al., "Hydro-geochemical and isotopic fluid evolution of the Los Azufres geothermal field, Central Mexico," *Applied Geochemistry*, vol. 20, no. 1, pp. 23–39, 2005.

[28] C. Siebe, F. Goff, M. A. Armienta, D. Counce, R. Poreda, and S. Chipera, "Geology and hydrogeochemistry of the Jungapeo CO_2-rich thermal springs, State of Michoacan, Mexico," *Journal of Volcanology and Geothermal Research*, vol. 163, no. 1-4, pp. 1–33, 2007.

[29] N. Kundu, M. Panigrahi, S. Sharma, and S. Tripathy, "Delineation of fluoride contaminated groundwater around a hot spring in Nayagarh, Orissa, India using geochemical and resistivity studies," *Environmental Geology*, vol. 43, no. 1-2, pp. 228–235, 2002.

[30] W. M. Edmunds, "Bromine geochemistry of British groundwaters," *Mineralogical Magazine*, vol. 60, no. 399, pp. 275–284, 1996.

[31] G. F. XU and Z. Y. MA, "Indication of strontium isotope for the deep geothermal Water," *Ground Water*, vol. 4, 2013.

[32] M. Zhang, Z. Guo, Y. Sano, Z. Cheng, and L. Zhang, "Stagnant subducted Pacific slab-derived CO_2 emissions: insights into magma degassing at Changbaishan volcano, NE China," *Journal of Asian Earth Sciences*, vol. 106, pp. 49–63, 2015.

[33] J. Liu, T. G. Li, and C. Duan, "Rb-Sr isochron dating and isotopic geochemistry characteristics of the Bajiazi large gold deposit, Jilin Province, China," *Acta Geologica Sinica*, vol. 92, no. 7, pp. 1432–1446, 2018.

[34] Y. Li, S. Qin, Y. Wang, G. Holland, and Z. Zhou, "Tracing interaction between hydrocarbon and groundwater systems with isotope signatures preserved in the Anyue gas field, central Sichuan Basin, China," *Geochimica et Cosmochimica Acta*, vol. 274, pp. 261–285, 2020.

[35] S. Q. Li, F. Chen, W. Siebel et al., "Late Mesozoic tectonic evolution of the Songliao basin, NE China: evidence from detrital zircon ages and Sr-Nd isotopes," *Gondwana Research*, vol. 22, no. 3-4, pp. 943–955, 2012.

[36] R. Karolytė, S. Serno, G. Johnson, and S. M. V. Gilfillan, "The influence of oxygen isotope exchange between CO_2 and H_2O in natural CO_2-rich spring waters: implications for geothermometry," *Applied Geochemistry*, vol. 84, pp. 173–186, 2017.

[37] G. Lu, X. Wang, F. Li et al., "Deep geothermal processes acting on faults and solid tides in coastal Xinzhou geothermal field, Guangdong, China," *Physics of the Earth and Planetary Interiors*, vol. 264, pp. 76–88, 2017.

[38] H. Craig, "Isotopic variations in meteoric waters," *Science*, vol. 133, no. 3465, pp. 1702-1703, 1961.

[39] M. Afsin, D. M. Allen, D. Kirste, U. G. Durukan, A. Gurel, and O. Oruc, "Mixing processes in hydrothermal spring systems and implications for interpreting geochemical data: a case study in the Cappadocia region of Turkey," *Hydrogeology Journal*, vol. 22, no. 1, pp. 7–23, 2014.

[40] X. Mao, Y. Wang, H. Zhan, and L. Feng, "Geochemical and isotopic characteristics of geothermal springs hosted by deep-seated faults in Dongguan Basin, Southern China," *Journal of Geochemical Exploration*, vol. 158, pp. 112–121, 2015.

[41] W. Z. Gu, Z. H. Pang, Q. J. Wang, and X. F. Song, "Isotope hydrology," in Science Press, Beijing, 2011.

[42] R. W. Henley and A. J. Ellis, "Geothermal systems ancient and modern: a geochemical review," *Earth-Science Reviews*, vol. 19, no. 1, pp. 1–50, 1983.

[43] W. Dansgaard, "Stable isotopes in precipitation," *Tellus*, vol. 16, no. 4, pp. 436–468, 1964.

[44] G. Lu and D. J. DePaolo, "Lattice Boltzmann simulation of water isotope fractionation during ice crystal growth in clouds," *Geochimica et Cosmochimica Acta*, vol. 180, pp. 271–283, 2016.

[45] Z. Mohammadi, R. Bagheri, and R. Jahanshahi, "Hydrogeochemistry and geothermometry of Changal thermal springs, Zagros region, Iran," *Geothermics*, vol. 39, no. 3, pp. 242–249, 2010.

[46] S. Arnorsson, E. Gunnlaugsson, and H. Svavarsson, "The chemistry of geothermal waters in Iceland. III. Chemical geothermometry in geothermal investigations," *Geochimica et Cosmochimica Acta*, vol. 47, no. 3, pp. 567–577, 1983.

[47] G. Lu, L. Huang, X. Chen, H. Hu, and X. Hu, "Guangdong Yangjing's Xinzhou's groundwater abnormal well Wwater relevant to deep geothermal system prior to and post Guangxi's Beiliu-Guangdong's Huazhou 2019 MS5.2 Earthquake," *South China Journal of Seismology*, vol. 40, no. 2, pp. 13–18, 2020.

[48] R. O. Fournier, "Chemical geothermometers and mixing models for geothermal systems," *Geothermics*, vol. 5, no. 1-4, pp. 41–50, 1977.

[49] R. O. Fournier, "A revised equation for the Na/K geothermometer," *Transactions of the Geothermal Resources Council*, vol. 3, pp. 221–224, 1979.

[50] R. O. Fournier and A. H. Truesdell, "An empirical Na *K* Ca geothermometer for natural waters," *Geochimica et Cosmochimica Acta*, vol. 37, no. 5, pp. 1255–1275, 1973.

[51] R. Nieva and R. Nieva, "Developments in geothermal energy in Mexico–part twelve. A cationic geothermometer for prospecting of geothermal resources," *Heat Recovery Systems and CHP*, vol. 7, no. 3, pp. 243–258, 1987.

[52] W. F. Giggenbach, R. Gonfiantini, B. L. Jangi, and A. H. Truesdell, "Isotopic and chemical composition of parbati valley geothermal discharges, North-West Himalaya, India," *Geothermics*, vol. 12, no. 2-3, pp. 199–222, 1983.

[53] R. O. Fournier, "Water geothermometers applied to geothermal energy," *Applications of Geochemistry in Geothermal Reservoir Development*, pp. 37–69, 1992.

[54] D. Canil and T. Lacourse, "Geothermometry using minor and trace elements in igneous and hydrothermal magnetite," *Chemical Geology*, vol. 541, article 119576, 2020.

[55] C. W. Karingithi, "Chemical geothermometers for geothermal exploration," *Short Course IV on Exploration for Geothermal Resources*, pp. 1–22, 2009.

[56] Q. Guo, Z. Pang, Y. Wang, and J. Tian, "Fluid geochemistry and geothermometry applications of the Kangding high- temperature geothermal system in eastern Himalayas," *Applied Geochemistry*, vol. 81, pp. 63–75, 2017.

[57] G. Lu and R. Liu, "Aqueous chemistry of typical geothermal springs with deep faults in Xinyi and Fengshun in Guangdong Province, China," *Journal of Earth Science*, vol. 26, no. 1, pp. 60–72, 2015.

[58] M. Reed and N. Spycher, "Calculation of pH and mineral equilibria in hydrothermal waters with application to geothermometry and studies of boiling and dilution," *Geochimica et Cosmochimica Acta*, vol. 48, no. 7, pp. 1479–1492, 1984.

[59] Z. Zhang, Z. Sun, and S. Wang, "Successful reconstruction the equilibrium status of Tanghu hot spring by using fixed-Al methods and it's meaningness," *Journal of East China Geological Institute*, vol. 26, no. 4, pp. 306–310, 2003.

[60] G. Jiang, S. Hu, Y. Shi, C. Zhang, Z. Wang, and D. Hu, "Terrestrial heat flow of continental China: updated dataset and tectonic implications," *Tectonophysics*, vol. 753, pp. 36–48, 2019.

[61] F. L. Gao, X. Q. Yang, G. A. Wu, Y. R. Fu, and Y. W. Chen, "Characteristics of thermal springs and genesis of thermal underground waters in Hainan Island," *Journal of Jilin University: Earth Science Edition*, vol. 39, no. 2, pp. 281–287, 2009.

[62] D. L. Parkhurst and C. A. J. Appelo, "User's guide to PHREEQC (Version 2): a computer program for speciation, batch-reaction, one-dimensional transport, and inverse geochemical calculations," *Water-resources investigations report*, vol. 99, no. 4259, p. 312, 1999.

[63] X. Mao, D. Zhu, I. Ndikubwimana, Y. He, and Z. Shi, "The mechanism of high-salinity thermal groundwater in Xinzhou geothermal field, South China: insight from water chemistry and stable isotopes," *Journal of Hydrology*, vol. 593, article 125889, 2021.